Université de Montréal

Quantitative ultrasound imaging during shear wave propagation for application related to breast cancer diagnosis

par

Marzieh Alavi Dorcheh

Institut de génie biomédical

Faculté de médicine

Mémoire présenté à la Faculté des études supérieures
en vue de l'obtention du grade de maîtrise ès sciences appliquées (M.Sc.A.)
en génie biomédical

Avril, 2014

Université de Montréal
Faculté des études supérieures

Ce mémoire intitulé:

Quantitative ultrasound imaging during shear wave propagation for application related to breast cancer diagnosis

présenté par:

Marzieh Alavi Dorcheh

a été évalué par un jury composé des personnes suivantes:

Farida Chériet,	président-rapporteur
Guy Cloutier,	directeur de recherche
Delphine Périé-Curnier,	membre du jury

Mémoire accepté le: . . . . . .

RÉSUMÉ

Dans le contexte de la caractérisation des tissus mammaires, on peut se demander ce que l'examen d'un attribut en échographie quantitative (« quantitative ultrasound » - QUS) d'un milieu diffusant (tel un tissu biologique mou) pendant la propagation d'une onde de cisaillement ajoute à son pouvoir discriminant. Ce travail présente une étude du comportement variable temporel de trois paramètres statistiques (l'intensité moyenne, le paramètre de structure et le paramètre de regroupement des diffuseurs) d'un modèle général pour l'enveloppe écho de l'onde ultrasonore rétrodiffusée (c.-à-d., la K-distribution homodyne) sous la propagation des ondes de cisaillement.

Des ondes de cisaillement transitoires ont été générés en utilisant la mèthode d' imagerie de cisaillement supersonique («supersonic shear imaging » - SSI) dans trois fantômes *in-vitro* macroscopiquement homogènes imitant le sein avec des propriétés mécaniques différentes, et deux fantômes *ex-vivo* hétérogénes avec tumeurs de souris incluses dans un milieu environnant d'agar-gélatine. Une comparaison de l'étendue des trois paramètres de la K-distribution homodyne avec et sans propagation d'ondes de cisaillement a montré que les paramètres étaient significativement ($p < 0,001$) affectès par la propagation d'ondes de cisaillement dans les expériences *in-vitro* et *ex-vivo*. Les résultats ont également démontré que la plage dynamique des paramétres statistiques au cours de la propagation des ondes de cisaillement peut aider à discriminer (avec $p < 0,001$) les trois fantômes homogènes *in-vitro* les uns des autres, ainsi que les tumeurs de souris de leur milieu environnant dans les fantômes hétérogénes *ex-vivo*. De plus, un modéle de régression linéaire a été appliqué pour corréler la plage de l'intensité moyenne sous la propagation des ondes de cisaillement avec l'amplitude maximale de déplacement du « speckle » ultrasonore. La régression linéaire obtenue a été significative : fantômes *in vitro* : $R^2 = 0.98$, $p < 0,001$; tumeurs *ex-vivo* : $R^2 = 0,56$, $p = 0,013$; milieu environnant *ex-vivo* : $R^2 = 0,59$, $p = 0,009$. En revanche, la régression linéaire n'a pas été aussi significative entre l'intensité moyenne sans propagation d'ondes de cisaillement et les propriétés mécaniques du milieu : fantômes *in vitro* : $R^2 = 0,07$, $p = 0,328$, tumeurs *ex-vivo* : $R^2 = 0,55$, $p = 0,022$; milieu environnant *ex-vivo* : $R^2 = 0,45$, $p = 0,047$.

Cette nouvelle approche peut fournir des informations supplémentaires à l'échographie quantitative statistique traditionnellement réalisée dans un cadre statique (c.-à-d., sans propagation d'ondes de cisaillement), par exemple, dans le contexte de l'imagerie ultrasonore en vue de la

classification du cancer du sein.

Mots clés: échographie quantitative, K-distribution homodyne, propagation d'ondes de cisaillement.

ABSTRACT

In the context of breast tissue characterization, one may wonder what the consideration of a quantitative ultrasound (QUS) feature of a scattering medium (such as a soft biological tissue) under propagation of a shear wave adds to its discriminant power. This work presents a study of the time varying behavior of three statistical parameters (the mean intensity, the structure parameter and the clustering parameter of scatterers) of a general model for the ultrasound backscattering echo envelope (i.e., the homodyned K-distribution) under shear wave propagation.

Transient shear waves were generated using the supersonic shear imaging (SSI) method in three *in-vitro* macroscopically homogenous breast mimicking phantoms with different mechanical properties, and two *ex-vivo* heterogeneous phantoms with mice tumors included in an agar-gelatin surrounding medium. A comparison of the range of the three homodyned K-distribution parameters with and without shear wave propagation showed that the parameters were significantly ($p < 0.001$) affected by shear wave propagation in the *in-vitro* and *ex-vivo* experiments. The results also demonstrated that the dynamic range of the statistical parameters during shear wave propagation may help discriminate (with $p < 0.001$) the three *in-vitro* homogenous phantoms from each other, and also the mice tumors from their surrounding medium in the *ex-vivo* heterogeneous phantoms. Furthermore, a linear regression model was applied to relate the range of the mean intensity under shear wave propagation with the maximum displacement amplitude of speckle. The linear regression was found to be significant : *in-vitro* phantoms : $R^2 = 0.98$, $p < 0.001$; *ex-vivo* tumors : $R^2 = 0.56$, $p = 0.013$; *ex-vivo* surrounding medium : $R^2 = 0.59$, $p = 0.009$. In contrast, the linear regression was not as significant between the mean intensity without shear wave propagation and mechanical properties of the medium : *in-vitro* phantoms : $R^2 = 0.07$, $p = 0.328$, *ex-vivo* tumors : $R^2 = 0.55$, $p = 0.022$; *ex-vivo* surrounding medium : $R^2 = 0.45$, $p = 0.047$.

This novel approach may provide additional information to statistical QUS traditionally performed in a static framework (i.e., without shear wave propagation), for instance, in the context of ultrasound imaging for breast cancer classification.

Keywords : Quantitative ultrasound, homodyned K-distribution, shear wave propagation.

CONTENTS

LIST OF TABLES

LIST OF FIGURES

LIST OF APPENDICES

LIST OF ABBREVIATIONS

MRI	Magnetic Resonance Imaging
QUS	Quantitative Ultrasound
ROI	Region of Interest
SSI	Supersonic Shear Imaging

To my parents.

ACKNOWLEDGMENTS

I would like to express my gratitude to my supervisor Prof. Guy Cloutier for his strong support during my M.Sc. research study, for his excellent guidance, patience, and motivation. My special thanks to Dr. François Destrempes for his valuable comments, continued supports combined with his kind efforts to bring this project to completion.

I would like to thank my master defense committee, Dr. Farida Chériet and Dr. Delphine Périé-Curnier ; I am grateful for their kind encouragement and insightful comments and guidance.

I would also like to extend my courtesy to the team at LBUM for their nice collaborations in a good chemistry environment, as well as for each of their individual expertise.

Finally, I would like to acknowledge the Natural Sciences and Engineering Research Council of Canada (NSERC # 365656-09) and the Canadian Institutes of Health Research (CPG-95288).

CHAPITRE 1

INTRODUCTION

Early screening and detection of small lesions and efficient follow-up are key issues for the optimal treatment of women afflicted by breast cancer. Needle biopsy is the gold standard for breast cancer diagnosis ; however, this is an invasive method. Furthermore, a lot of irrelevant biopsies are performed each year. Therefore, medical imaging methods have been used to reduce the number of non-necessary biopsies. These methods are categorized with the following three modalities : X-ray mammography, magnetic resonance imaging (MRI) and ultrasound echography. Mammography reduces breast cancer mortality, but the image contrast is reduced in young women because of the high breast parenchyma density. Moreover, it cannot determine the nature of lesions. The highest resolution among the three mentioned modalities belongs to MRI, but the application of MRI is limited due to its high cost and time consuming acquisition procedure. Ultrasound imaging with no radiation has been known as a complete non-invasive method in breast cancer diagnosis. It is widely available and relatively cheap but has a lower resolution and is operator dependent. The preoperative assessment of breast cancer most often requires to combine mammography, MRI and ultrasound imaging because of their respective limitations, which increases the health care costs and time of diagnosis. It is thus clear that new developments in medical imaging analysis techniques are required to detect breast tumors and determine the nature of lesions ; i.e., to differentiate between malignant and benign tumors. The purpose of this study is to propose a new approach in ultrasound image processing to provide additional information with potential application in breast lesion detection and classification.

Quantitative methods such as quantitative ultrasound (QUS) and dynamic elastography have been developed to improve the accuracy of ultrasound imaging. Significant differences have been observed in the microstructure of breast pathological tissues. Quantitative ultrasound provides information about the microstructure of tissues, such as cell organization, which may help distinguish between a pathological tissue and a healthy tissue. Different statistical QUS distributions have been proposed to model the ultrasound echo envelope. The homodyned K-distribution is a general statistical distribution with physically interpretable parameters. From another point of view, a stiffer tissue may be an early warning in breast cancer diagnosis. Therefore, elastography methods have been used to estimate tissue viscoelasticity in order to categorize pathological and

normal tissues. Ultrasound dynamic elastography assesses the mechanical properties of tissue through shear wave propagation and detection of the tissue displacement. More sophisticated QUS and dynamic elastography methods are needed to improve breast cancer diagnosis.

Different types of information are obtained from QUS and dynamic elastography. This project proposes a novel approach in QUS to understand the behavior of ultrasound scatterers under shear wave propagation. The main objective is to assess the time evolution of statistical QUS parameters under shear wave propagation in order to obtain additional information for tissue characterization. In this study, five hypotheses are evaluated to achieve the main objective. It is first hypothesized that the homodyned K-distribution parameters estimated from ultrasound echo envelope data are affected by shear wave propagation. The second hypothesis states that the difference between the maximal and minimal values of the homodyned K-distribution parameters during shear wave propagation can be used to differentiate between different tissue mimicking phantoms. The third hypothesis is related to the correlation between the maximal displacement amplitude of the medium in the phantoms or the reciprocal of the Young's modulus with the range of the parameters of the homodyned K-distribution during shear wave propagation in the *in-vitro* experiments. The fourth hypothesis, which is evaluated with *ex-vivo* experiments on mice tumors, demonstrates that the difference between the maximal and minimal values of the homodyned K-distribution parameters during shear wave propagation can help to distinguish the mice tumors from their surrounding medium. Finally, correlations between the maximal displacement amplitude of the medium in the mice tumors with the range of the parameters of the homodyned K-distribution during shear wave propagation are examined in the last hypothesis.

The main body of this thesis is separated into five chapters. Following the introduction, the second chapter presents a literature review and background. This chapter contains an overview of non-invasive clinical methods used in breast cancer diagnosis. Then, ultrasound imaging and its main challenges in breast cancer diagnosis are explained. The rationale for QUS and elasticity imaging are also presented. A review on ultrasound echo envelopes and elasticity imaging methods is presented. The third chapter presents the methodology used in this research study. It starts with the hypotheses of the current study and a general overview of the experiments corresponding to each hypothesis. Next, it continues with experimental procedures in the *in-vitro* and *ex-vivo* experiments. The data analysis to estimate the homodyned K-distribution parameters during shear wave propagation is presented as well. Chapter four presents the results obtained from the post processing of the experimental data. The results are classified into five sections regar-

ding mentioned hypotheses. The feasibility of considering QUS under shear wave propagation as a new approach in ultrasound imaging is evaluated. The last chapter presents a discussion and a conclusion. In this chapter, the results are explained with more details and the limitations of the study are presented. Finally, future works are discussed as a perspective of this study. The appendix section includes two published conference papers that include preliminary results related to this study.

CHAPITRE 2

LITERATURE REVIEW AND BACKGROUND

2.1 Significance of the study : Breast cancer statistics and clinical diagnostic methods

According to the National Cancer Institute of Canada, breast cancer is the most common cancer among Canadian women. In 2012, an estimated 22,700 women were diagnosed and 5,100 died of breast cancer in Canada. Statistically, an average of 14 women die of breast cancer every day. Early diagnosis and detection of smaller tumors are key issues in optimal treatment (10).

Clinical breast exam (CBE) is a medical examination performed by trained professionals for early diagnosis of breast cancer (23). The CBE-detected suspicious breast lesions can be further examined using different breast screening methods such as mammography. Needle biopsy is used to take tissue samples for pathological examination, in order to assess the malignancy. The clinical methods for breast cancer diagnosis are reviewed in the following sections.

2.1.1 Non-invasive imaging modalities

The non-invasive diagnostic methods for breast cancer, which are used by clinicians are categorized into three groups : X-ray mammography, magnetic resonance imaging (MRI) and ultrasound imaging.

2.1.1.1 Mammography

Mammography is recommended for annual screening of women beginning at age 40 (24), (5). Mammography has reduced breast cancer mortality (61), especially in women over the age of 50 by 25-30% (54), however, it is less effective for young women (18). The image contrast in this method is low for high density breasts and needs an additional mammography view or ultrasound (31), which increases the cost of health care (70). Moreover, some studies have shown that the results of mammography screening depend on the menstrual cycle of women (69) and their hormonal status (35). This method is unable to distinguish between benign and malignant tumors (27), (49).

2.1.1.2 MRI

The American Cancer Society suggests women with approximately a 20% or greater lifetime risk of breast cancer to have MRI screening (53). MRI has higher sensitivity compared to mammography and it is recommended for high risk young women after having mammography (68) , (36) , (32). On the other hand, the specificity of this method in the evaluation of breast lesions is still not very high, about 72% (48). It is also time consuming and uncomfortable due to intravenous injection of gadolinium. Furthermore, it is an expensive technique (25). Moreover, MR elastography (MRE) was proposed to estimate viscoelastic shear properties of tissues (47). Clinical applications of MRE to breast lesions showed that this imaging method could increase the specificity of the current MRI technique by visualization of mechanical properties of breast tissues (58), but with the disadvantage of a longer acquisition time.

2.1.1.3 Ultrasound imaging

Ultrasound imaging is an inexpensive and more comfortable modality, which is completely non-invasive with no radiation. Thus, it can be used as a complementary test to mammography (6), (4). It is also able to differentiate between cysts (fluid) and solid masses (37). However, the specificity of the combination of mammography and ultrasound is relatively low, which means that the number of false positives can exceed the true positives (19). Other limitations of ultrasound echography are its low resolution and operator dependency.

2.1.1.4 Synthesis

Several studies have compared the three mentioned imaging methods for breast cancer detection. The results show that most often it is required to combine mammography, MRI and ultrasound to improve the accuracy of medical imaging (18), which increases health care costs. Moreover, a large number of irrelevant biopsies are conducted each year because of the low specificity of current diagnostic imaging methods (39). Therefore, new improvements in clinical imaging modalities are required for precise detection of breast tumors, to determine the nature of lesions (i.e., to differentiate between malignant and benign tumors) and to reduce the number of irrelevant biopsies.

2.1.2 BI-RADS classification

According to pathological studies, there are different types of breast lesions. Breast lesions are categorized into benign (non-cancerous) and malignant (cancerous) types. In addition to breast lesion detection, the imaging modalities aim to classify breast lesions into benign or malignant. Breast imaging-reporting and data system (BI-RADS) has been developed by the American College of Radiology. The BI-RADS score provides a standardized classification to demonstrate the probability of breast malignancy. As the score increases from 0 to 6, the probability of cancer increases. Table 2.I shows BI-RADS categories and the interpretation for each score. No biopsy is recommended in the case of BI-RADS 0-3, while BI-RADS 4-5 leads patients to take a biopsy (59).

TABLE 2.I – BI-RADS categories.

BI-RADS score	Definition
0	need additional imaging evaluation
1	negative
2	benign finding
3	probably benign
4	suspicious abnormality
5	highly suggestive of malignancy
6	known biopsy-proven malignancy

Ultrasonographic characteristics of benign and malignant breast lesions have been used to determine BI-RADS scores (37). Table 2.II shows some of the ultrasonographic features used for breast lesion classification.

TABLE 2.II – Ultrasonographic characteristics for breast lesion classification.

Ultrasonographic characteristics	Benign	Malignant
Shape	round, oval	irregular
Margin	circumscribed	indistinct
Lesion boundary	abrupt interface	echogenic halo
Echogenicity	hyperechoic, homogeneous	hypoechoic, inhomogeneous
Acoustics features	no posterior acoustic features	shadowing

As an example, Figures 2.1 and 2.2 show two ultrasound images from a fibroadenomas (benign) and a carcinoma (malignant), which are two common breast lesion types among women. Considering Table 2.II, the images can be differentiated. However, the qualitative criteria are not certain and the benign and malignant images can be similar (60).

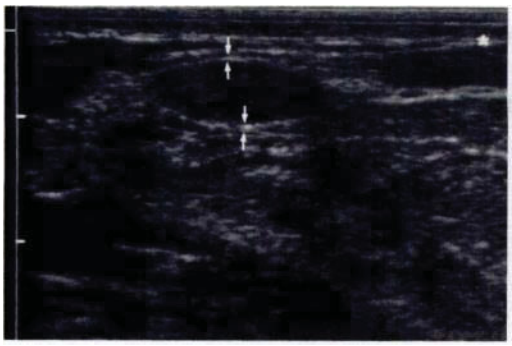

FIGURE 2.1 – The B-mode image of a benign breast lesion (fibroadenoma) (60).

FIGURE 2.2 – The B-mode image of a malignant breast lesion (carcinoma) (60).

2.1.3 The role of needle biopsy and ultrasound data analysis in breast cancer diagnosis

The gold standard method in breast cancer detection is needle biopsy. As mentioned before, the number of irrelevant biopsies indicates the importance of improving the clinical imaging modalities. In breast ultrasound imaging, low resolution images and operator dependency of the ultrasound echography increase the complexity of breast lesion classification. All these challenges emphasize the need for developing more sophisticated methods in data analysis to provide quantitative criteria for breast lesion classification. In the following sections, two different approaches are introduced for quantitative breast lesion classification after a brief overview on the physics of ultrasound.

2.2 Principles of ultrasound imaging

Ultrasound is an acoustic wave with frequencies ranging from 20 kHz up to several GHz, which is greater than the range of human hearing. As a medical imaging modality, ultrasound can propagate through the human body to produce an image of different organs and tissues. Different interactions of ultrasound waves with tissues include reflection, refraction, scattering, and absorption (8).

The reflection of ultrasound wave takes place at the boundary of two tissues with different acoustic impedances. In general, a fraction of an incident wave is transmitted to the second me-

dium and a fraction is reflected back to the first medium. The schematic of ultrasound interaction with a simple plane boundary between two tissues with different acoustic impedance is presented in Figure 2.3.

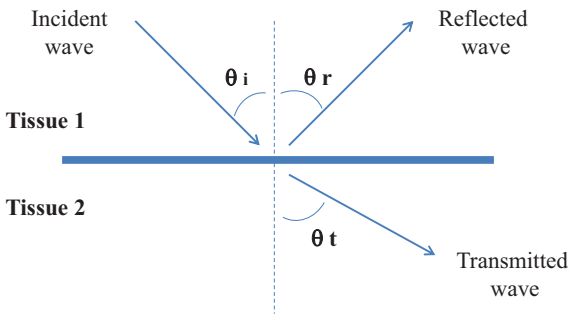

FIGURE 2.3 – Specular reflection and refraction of an incident ultrasound wave occurs at tissue boundaries with different acoustic impedances (8).

Ultrasound refraction happens when the incident beam is not perpendicular to the boundary. In this case, the direction of the transmitted ultrasound wave is changed. The refraction angle, θ_t, follows the Snell's law equation :

$$\frac{sin(\theta_i)}{sin(\theta_t)} = \frac{c_2}{c_1}, \tag{2.1}$$

where θ_i is the incident angle, c_1 and c_2 are the speed of sound in the first and second media, respectively, and θ_r is the reflection angle.

The ultrasound wave may scatter in many directions when reaching a boundary with a smaller dimension than the wave length (λ). The behavior of the ultrasound wave at boundaries depends on their characteristics. Figure 2.4 shows different types of ultrasound wave interactions at boundaries (8).

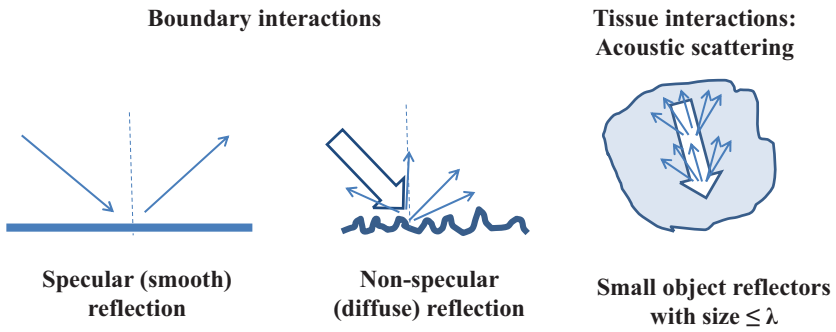

FIGURE 2.4 – Ultrasound interactions with boundaries and particles (8).

The loss of acoustic energy during the ultrasound wave propagation in the tissue is called attenuation. Scattering and tissue absorption are the two main sources of attenuation. The attenuation increases with the frequency and also increases exponentially with the penetration depth.

The ultrasound image is created by transmitting the acoustic wave into the medium and collecting the reflected echoes. Three different modes have been used to display the ultrasound echo, namely A-mode, B-mode and M-mode. The A-mode shows the amplitude of the reflected wave as a function of time. This mode is currently used for ophthalmology. The B-mode image is composed of brightness-modulated dots, which are constituted from the A-mode images. The gray scales in the two dimensional B-mode images are interpreted as the echo signal amplitude. Finally, the M-mode images are obtained from a technique, which makes a movie from the moving organs by combining the B-mode images. The M-mode is not commonly used after the developments of Doppler imaging.

2.3 Quantitative methods in ultrasound tissue characterization

As reviewed in previous sections, ultrasound imaging is inexpensive and has no radiation. It is also a fast screening method, but the main restriction of ultrasound is its low resolution and operator dependency. Quantitative ultrasound and dynamic elastography are two different approaches used for establishing quantitative criteria to distinguish the pathological tissues, which are discussed in the following sections.

2.3.1 Quantitative ultrasound

Quantitative ultrasound (QUS) was introduced a few decades ago (9) ,(33). The hypothesis underlying statistical QUS is that the spatial organization of the cell nuclei and their scattering properties can be detected by the statistical parameters (46). A significant difference in the micro structure of breast pathological tissues has been documented in the literature (45). Figure 2.5 shows the optical photo micrographs of breast tissues in mice. Based on these observations, the difference in diameter or acoustic concentration of cells and nuclei (playing the role of scatterers) can lead to the classification of pathological breast tissues (45).

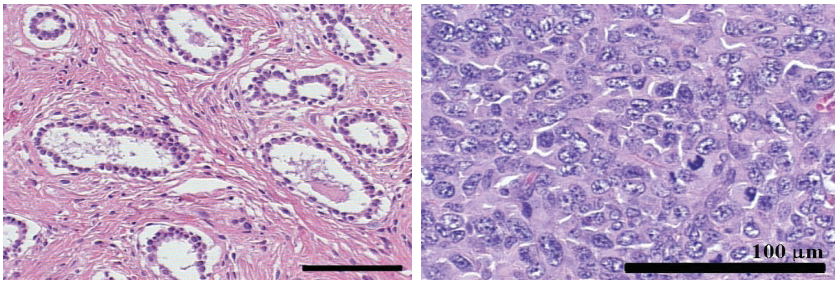

(a) **(b)**

FIGURE 2.5 – Light microscopy comparisons of breast lesions in mice. (a) fibroadonemas (benign), (b) carcinomas (malignant) (45)

.

2.3.1.1 Distribution models for ultrasound echo envelope

In ultrasound imaging, there are different models, which were proposed for the first-order statistics of the echo envelope of a B-mode image. An ideal statistical distribution model for tissue characterization fits very well with experimental data. Additionally, the parameters used for tissue classification should have a physical meaning.

Among different models that were used in tissue characterization, the main models with physically interpretable parameters are presented in Figure 2.6. In these models, α is interpreted as the scatterer clustering parameter (17) or the effective density of the scatterers (57). The effective density is defined as the number of random scatterers per resolution cell (N) multiplied by a coefficient called homogeneity (α_0). The coherent signal component is another parameter, which is

shown by ε. For the case of a macroscopically homogenous medium with no periodic scatterers, the parameter ε vanishes.

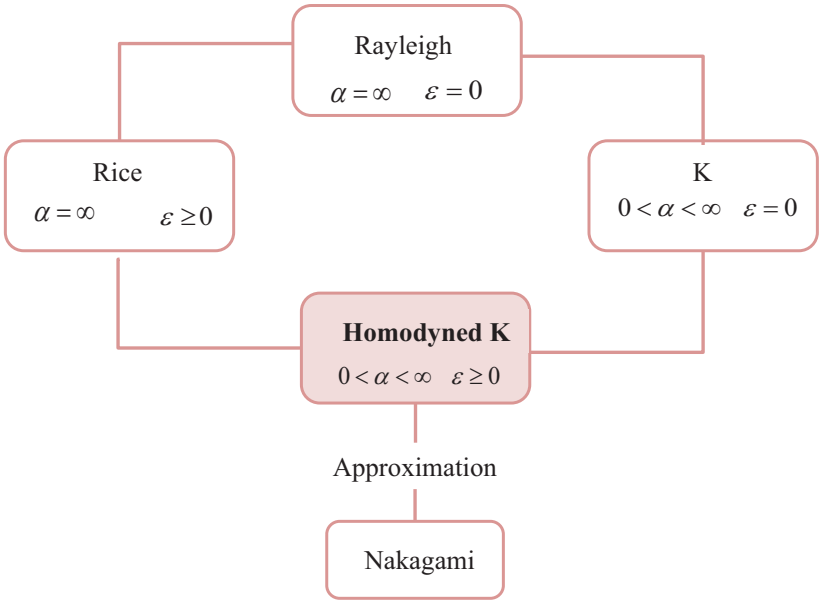

FIGURE 2.6 – The most applicable distribution models for ultrasound echo envelope in biomedical applications.

According to Figure 2.6, the Rayleigh distribution, introduced in 1880, is the most specific case (50) in ultrasound echo envelope models with the assumption of high effective density of random scatterers (67). The Rice distribution is another model, which is also applicable for high density of scatterers. On the other hand, it considers the presence of coherent signal component ($\varepsilon \geq 0$) (12).

The homodyned K-distribution is a general model in ultrasound echo envelope modeling and amounts to the K-distribution in the absence of the coherent signal component (28), (29). Compared to the Rayleigh model, the K-distribution fits better with the envelope of the backscatter radio-frequency (RF) data from breast tissues (57), (40).

The estimation of the homodyned K-distribution parameters is challenging and rarely used in the literature on QUS (26). In order to simplify the analytical procedure, the Nakagami distribution, as an estimation of the homodyned K-distribution, was used by Shankar in tissue characterization (55). This model was first introduced by Nakagami in the field of wave propagation in

1943 (42). The Nakagami model has been widely used in tissue characterization as well as breast tissue classification due to its simplicity and its potential to encompass different scattering conditions (56), (65), (16). Moreover, it is shown that a Nakagami parametric imaging could combine with the B-mode image to provide a better visualization of the structure of the tissues (64), (15).

The above studies mainly concerned the discrimination of benign breast lesions from malignant with no attention to BI-RADS classification. A recent study showed the potential of the homodyned K-distribution in breast lesion classification in order to avoid biopsy, while not missing malignant tumors (63).

2.3.1.2 Homodyned K-distribution

In the context of random walks and non-Gaussian scattering modeling, the homodyned K-distribution was proposed. For ultrasound imaging application, the homodyned K-distribution model presents three parameters that have physical meanings.

Assume A is the amplitude of an ultrasound backscattering signal, $\varepsilon \geq 0$ is the coherent signal component, $\sigma^2 > 0$ is related to the diffuse signal power and $\alpha > 0$ is the effective density of the scatterers, the two-dimensional homodyned K-distribution is demonstrated as the following equation :

$$P(A \mid \varepsilon, \sigma^2, \alpha) = A \int_0^\infty u J_0(u\varepsilon) J_0(uA) \left(1 + \frac{u^2\sigma^2}{2}\right)^{-\alpha} du, \tag{2.2}$$

where, J_0 is the Bessel function of the first kind of order 0.

In this work, the homodyned K-distribution was used to estimate the ultrasound echo envelope from breast tissue mimicking phantoms.

2.3.2 Elasticity imaging

For centuries, physicians have utilized palpation as an important diagnostic tool. The ubiquitous presence of a *stiffer* tissue associated with pathology often represents an early warning sign of breast cancer. The mechanical parameters, which are characterized by palpation are determined by Young's modulus (E) or shear modulus (G) (22).

Elastography is a method to determine the mechanical properties of materials. During the past 20 years, different elastography techniques have been adopted to estimate tissue elasticity in order to categorize pathological and normal tissues (47).

In static elastography, the tissue is deformed by applying pressure (stress) and measuring the deformation (strain). The Young's modulus can be retrieved by the following ratio :

$$E = \frac{\sigma}{\varepsilon}, \tag{2.3}$$

where σ is the applied stress and ε is the measured strain. Figure 2.7 shows the physical concept of static elastography. The hard inclusion represents the malignant tumor while the soft inclusion represents a benign lesion in a surrounding tissue. By applying the pressure, the soft inclusion is deformed more than the hard one. On the other hand, the Young's modulus of the pathological tissue is statistically higher in comparison to the normal tissue. Two-dimensional map of the Young's modulus (elasticity) is called elastogram, which is presented with a color-bar. This method is limited due to its operator dependency and the non-uniformity of the pressure applied (47).

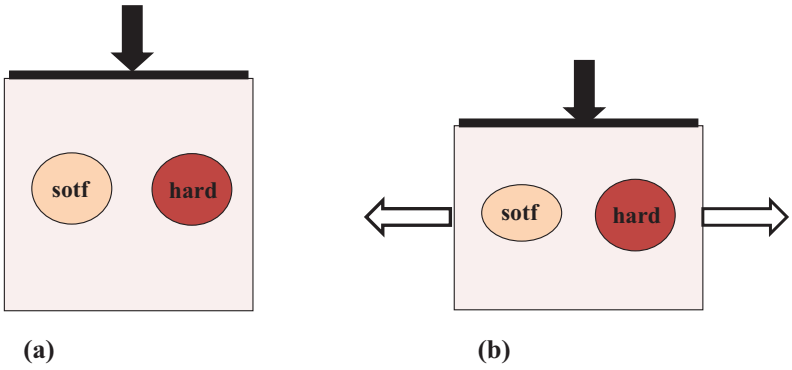

FIGURE 2.7 – The principle of static elastography. (a) The heterogeneous medium with two inclusions (one inclusion is softer and another is harder compared to the surrounding medium) is shown before applying the stress. (b) After applying the stress, the soft and hard inclusions have different responses.

To avoid the limitations of static elastography, ultrasound dynamic elastography was introduced (52). In this method, shear waves are propagated in the medium using an internal or external excitation and the medium displacement is detected with ultrasound imaging. As seen in Figure 2.8, when the excitation is applied, each particle moves in the Y direction while shear wave

propagates in the X direction.

Consider ρ as the density of the medium, the shear modulus is related to the plane shear wave velocity (c_s) by the following equation (22) :

$$G = \rho c_s^2. \tag{2.4}$$

In the case of biological tissues, which are mostly incompressible, the shear modulus becomes :

$$G \to E/3. \tag{2.5}$$

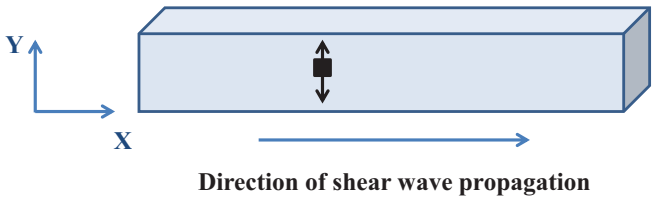

FIGURE 2.8 – Shear wave propagation in the medium. The black square represents a particle of the medium. The particle motion is perpendicular to the direction of wave propagation.

The addition of an elasticity modulus to ultrasound echography may improve the ability of this method for breast cancer diagnosis and lesions classification (7).

Figure 2.9 shows an overview of the methods used in elasticity measurement. As it is indicated, to estimate the mechanical properties, a tissue is deformed with a static or dynamic excitation that can be applied by an external or internal source. The next step is to image the tissue response with a mechanical, optical, MRI or ultrasound imaging technique. Finally, the mechanical properties can be estimated qualitatively and quantitatively. It is important to note that in the current work, the estimated parameters are the homodyned K-distribution parameters during the shear wave propagation. Therefore, the highlighted parts in Figure 2.9 demonstrate the experimental procedure used in this study to generate a shear wave inside the medium and collect the data to estimate the statistical and mechanical parameters during shear wave propagation.

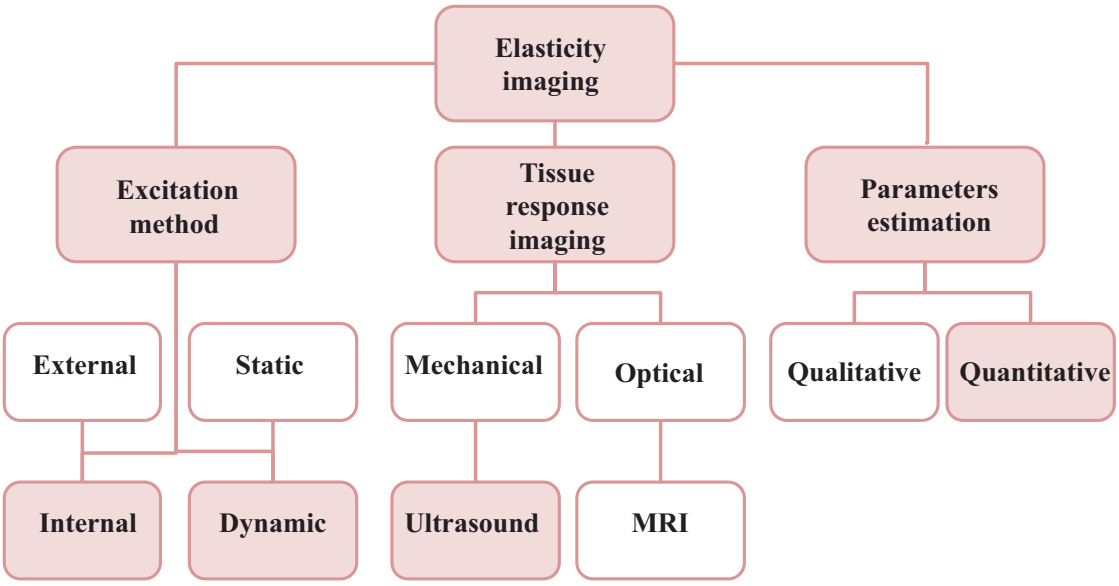

FIGURE 2.9 – Different techniques in elastography for measuring the mechanical properties of the biological tissue (the diagram is adopted from (38)).The highlights demonstrate the method of the current dissertation to estimate the statistical and mechanical properties of the phantoms.

In this dissertation, the tissue mimicking phantoms were excited with supersonic shear imaging as an internal excitation method to produce shear waves. The phantom responses were imaged with a fast imaging technique (plane wave imaging). These two methods are discussed in the following parts. Finally, the method to estimate the displacement map is explained in the last section.

2.3.2.1 Supersonic shear imaging

Supersonic shear imaging (SSI) is a recent technique in ultrasound dynamic elastography that visualizes elasticity of soft tissues. In this method, shear waves are produced by acoustic radiation force. The radiation force is a highly focused ultrasound beam that can remotely vibrate tissue and produce shear wave propagation. The physics of SSI is similar to the phenomenon that happens with a supersonic aircraft. A Mach cone is produced by different pushing beams at different depths. There is a time delay between the bursts. The Mach cone and the direction of shear wave propagation are in Figure 2.10.

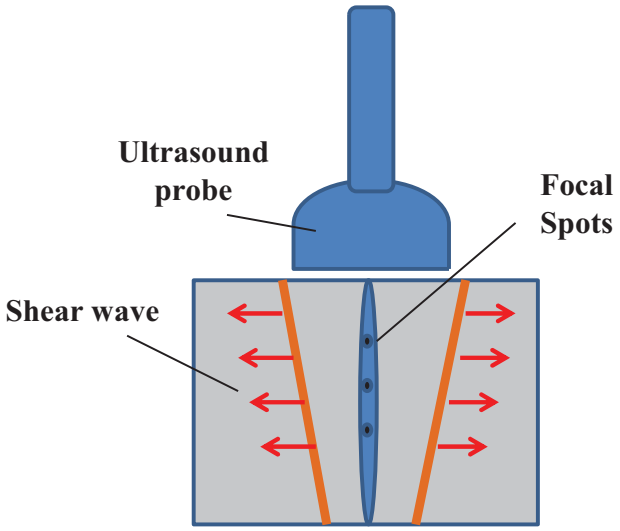

FIGURE 2.10 – Producing the plane shear wave with SSI method.

2.3.2.2 Plane wave imaging and migration method

Plane wave imaging (PWI) is a recent technique in ultrasound imaging that provides ultra-fast imaging with a high frame rate. In this method, by a single transmit a full image can be acquired. A point ultrasound scatterer acts as a spherical wave emitter when the plane wave interacts with it (Figure 2.11). Therefore, a spherical wave travels upwards and a hyperbolic curve is produced from echoes received by each transducer element (Figure 2.12).

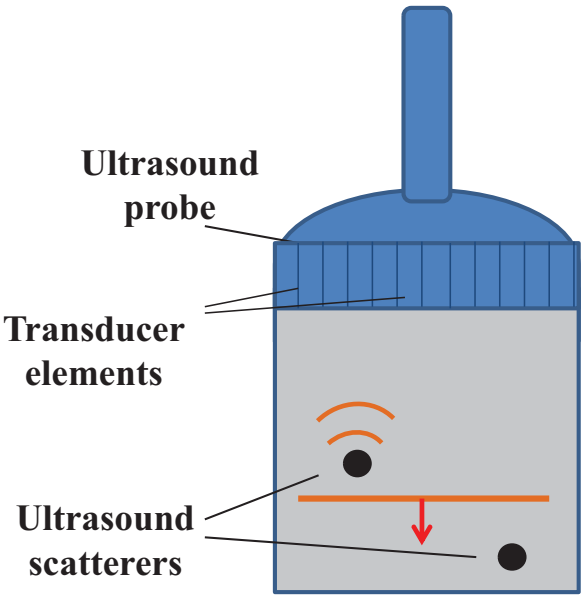

FIGURE 2.11 – A scatterer acts as a second source in the plane wave imaging method (20).

To have a high quality B-mode image, the diffracted hyperbola should migrate back to their apexes (migration process). Different migration algorithms were used in this field. In this work, the migration algorithm used is called frequency-wave number (*f-k*) method (20). The choice of this method is due to its benefits such as fast computation and high contrast to noise ratio. It is important to mention that no compression was applied on the reconstructed B-mode images when the Hilbert transform was used to convert the RF signals to the B-mode images.

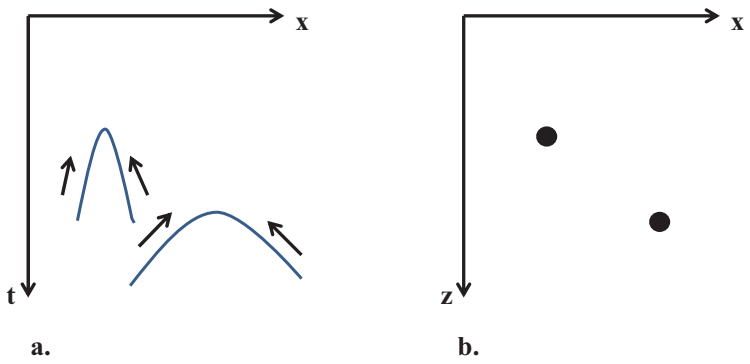

FIGURE 2.12 – a. RF migration lines as parabolic curves in the time domain from two point scatterers are shown. b. The migrated image after applying the migration process and the reconstruction are presented. The position of the point scatterers were recovered (20).

2.3.2.3 Displacement map

A one-dimensional normalized cross-correlation algorithm was applied on the RF data to estimate the displacement map (41). Technically, a graphical processor unit (GPU) can be used to faster computation speeds compared to a single processor unit (CPU).

CHAPITRE 3

METHODOLOGY

The materials and methods used in the current project are described in this chapter. First of all, the hypotheses are presented. To evaluate these hypotheses, *in-vitro* and *ex-vivo* experiments were considered. The experimental procedure for making the phantoms and collecting the radio frequency (RF) data are explained in the following section. The data analysis to estimate the parameters of the homodyned K-distribution during shear wave propagation are presented in the next step.

3.1 Static QUS and dynamic QUS

Based on the literature, statistical QUS parameters are estimated from ultrasound images of biological tissues without shear wave propagation (13). However, it is shown that by compressing breast tissue, the estimation of statistical QUS parameters can improve the tissue classification (34). The estimated QUS parameters reveal information about size, density, structure and acoustical properties of the scatterers and the of ambient medium. The purpose of this work is to study the dynamic behavior of statistical parameters of an ultrasound echo envelope model by performing QUS analysis under shear wave propagation. The main question of this study is as follows :

Can the dynamic behavior of the statistical echo envelope parameters provide extra information on the microstructural analysis of the scatterers revealed by QUS ?

In this dissertation, static QUS is defined as QUS without shear wave propagation, and dynamic QUS as QUS during shear wave propagation (Figure 3.1). In static QUS, the estimated parameters may be reported as the median (or the mean value in the case of many images) of the statistical parameters in a sequence of images (14). In dynamic QUS, we propose studying the range (max-min) of the estimated parameters during shear wave propagation. Note that in the case of static QUS, the range of the statistical parameters is expected to be near zero as no shear wave is propagating. Also, since the shear wave is rapidly attenuated with the SSI method, the median value of the estimated parameters in the case of dynamic QUS would be redundant with the median value in static QUS.

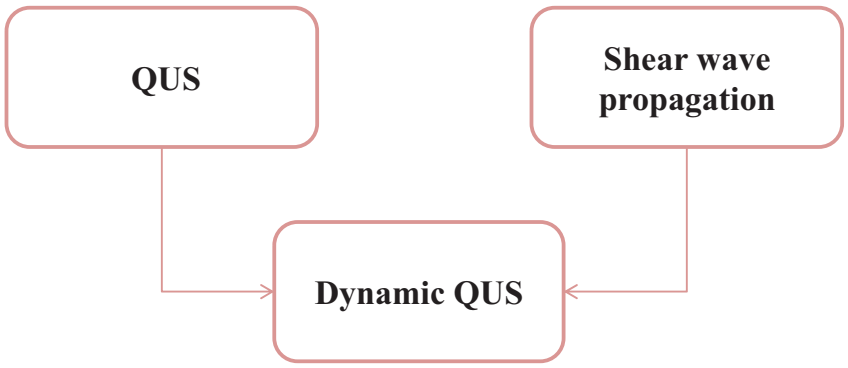

FIGURE 3.1 – Definition of dynamic QUS.

3.2 Hypotheses and overview of the experiments

Five hypotheses are studied in this research by means of two sets of experiments (*in-vitro* and *ex-vivo*). Figure 3.2 shows an overview of the experiments to investigate the hypotheses of the project. *In-vitro* experiments were used to evaluate hypotheses 1 to 3 and *ex-vivo* experiments were used to examine the last two hypotheses.

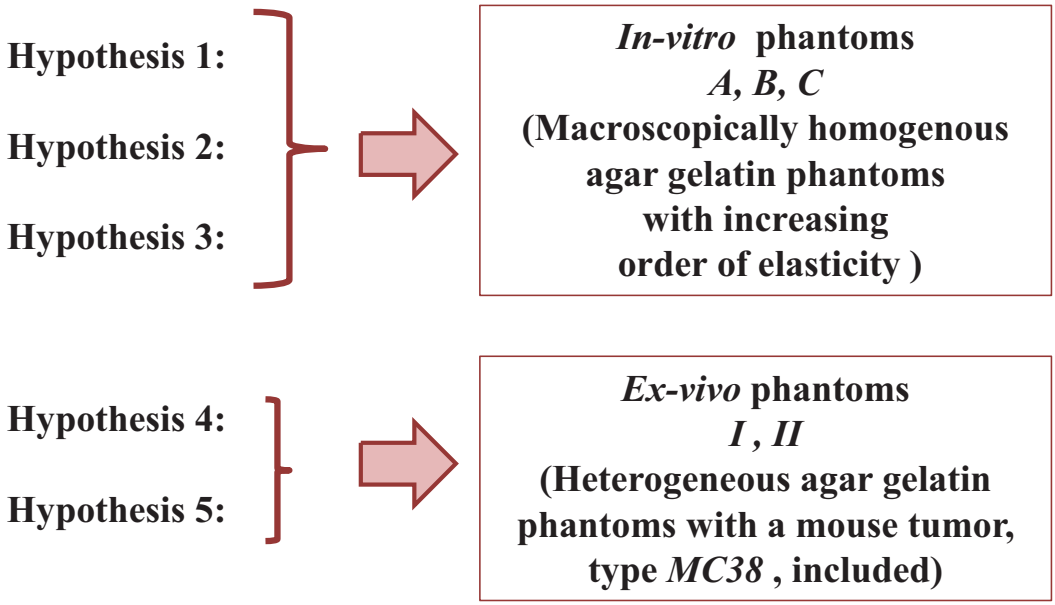

FIGURE 3.2 – Overview of the experiments corresponding to the hypotheses.

3.2.1 *In-vitro* experiments

Any variation in sound speed produces acoustic scattering. To avoid the complexity of scattering effects of the ultrasound beam from the mimicked breast lesion boundaries during shear wave propagation in heterogeneous media, macroscopically homogenous phantoms were studied for the first three hypotheses (*in-vitro* measurements).

Hypothesis 1 : The parameters of the homodyned K-distribution from ultrasound echo envelope data are affected by shear wave propagation.

Hypothesis 2 : The range (max-min) of the parameters of the homodyned K-distribution during shear wave propagation can be used to discriminate different tissue mimicking phantoms.

Hypothesis 3 : The maximal displacement amplitude of the medium and the reciprocal of the Young's modulus are correlated with the range of the parameters of the homodyned K-distribution during shear wave propagation.

3.2.2 *Ex-vivo* experiments

Having shown the effect of shear wave propagation on the statistical parameters of the ultrasound echo envelope with the *in-vitro* experiments, the next step was to explore the effect of shear wave propagation on the mice tumors and to discriminate the mice tumors from their surrounding medium with dynamic QUS. Here, two agar gelatin phantoms were used. A mouse tumor was placed inside the agar gelatin phantom as an inclusion to mimic pathological breast tissues. The discrimination ability of dynamic QUS to differentiate between the tumors and their surrounding media were evaluated. The two final hypotheses are presented as follows :

Hypothesis 4 : Dynamic QUS can help in distinguishing the mice tumors from their surrounding medium.

Hypothesis 5 : The maximal displacement amplitude of the mice tumors is correlated with the range of the parameters of the homodyned K-distribution during shear wave propagation.

3.3 Phantom fabrication

A brief overview of the fabrication process for the homogenous (*in-vitro*) and the heterogeneous (*ex-vivo*) phantoms is presented in this section. A wide range of elasticities are reported for breast tissues. Table 3.I shows the range of Young's modulus of breast lesions in four studies published in the past decade. The reported values vary according to the types of breast lesions included in the studies and the measuring techniques used.

TABLE 3.I – Ranges of Young's modulus of breast lesions corresponding to four studies.

Reference	Range of the Young's modulus E (k Pa)
Samani et al. 2007 (51)	3.24 ± 0.61 to 42.52 ± 12.47
Tanter et al. 2008 (62)	62.50 ± 24.75 to 140.00 ± 56.57
Chang et al. 2011 (11)	46.1 ± 42.9 to 153.3 ± 58.1
Umemto et al. 2014 (66)	2.60 ± 0.59 to 16.08 ± 9.06

Agar gelatin phantoms with different proportions of agar and gelatin were used to mimic the mechanical properties of breast lesions (21). To build the agar gelatin phantoms, water at 80 degree Celsius was mixed with gelatin (Sigma Chemical, number G-2500 type A from porcine

skin, Saint-Louis, MO, USA) and agar powder (Sigma Chemical, number A-6924, Saint-Louis, MO, USA) as the ultrasound scatterers. The gelatin played the role of a matrix containing the scatterers.

The proportions of the agar and gelatin for the three homogenous phantoms and their corresponding Young's modulus are listed in Table 3.II. As one can see, the elasticity of the phantoms are increasing from phantom *A* to *C* and these elasticities are within the range of Young's modulus of various breast lesions that are reported in (51).

TABLE 3.II – Macroscopically homogenous agar gelatin phantoms and their corresponding Young's modulus.

Name of the phantom	*A*	*B*	*C*
Proportion of agar-gelatin	$2\% - 3\%$	$2\% - 4\%$	$3\% - 3\%$
E (k Pa)	17.52	21.76	44.05

For the *ex-vivo* phantoms, a mouse tumor (from *MC38* cells) was used as an inclusion inside the agar gelatin phantoms. The *MC38* cells are mice colon cancer cells. To obtain *MC38* tumors, wild type synergistic *C57Bl/6* mice were injected subcutaneously with 1 million *MC38* cells in 100 micro liter of phosphate buffered solution (PBS) and the tumors were harvested on the day 25 after euthanasia (3). Here the surrounding material for the heterogeneous phantoms was 3% agar and 3% gelatin (Figure 3.3).

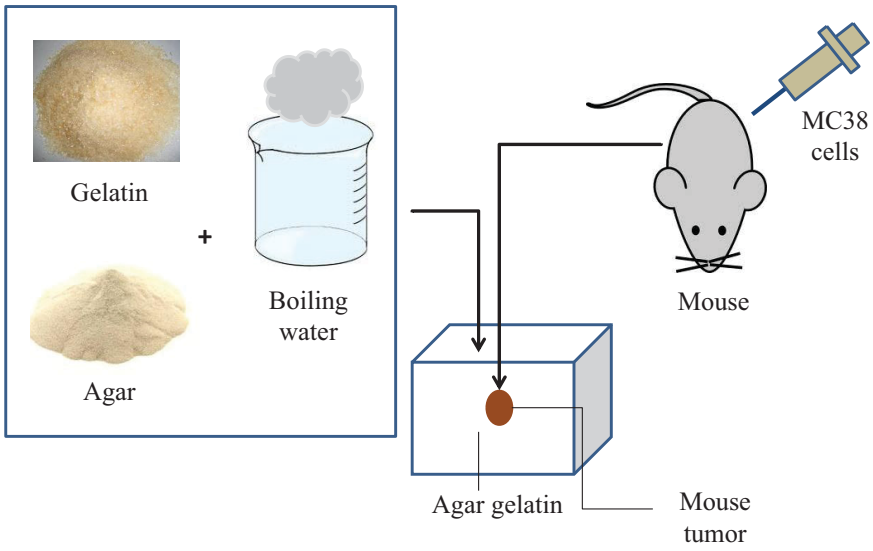

FIGURE 3.3 – Heterogeneous phantom fabrication with the mouse tumor.

3.4 Experimental procedure

Shear waves were generated in the phantoms with the SSI method. The plane wave imaging technique was used to acquire the RF data during shear wave propagation. The experimental set-up of the experiments is described in the following subsections.

3.4.1 *In-vitro* measurements

Figure 3.4 shows a schematic diagram of the experimental set-up. A Verasonics system (Verasonics Inc, Redmond, WA, USA) was used to generate the acoustic radiation force as a remote source of shear waves. The ultrasound probe (Philips Healthcare, Andover, MA (L7-4)) with a 5 MHz central frequency was an array including 128 transducer elements. The probe width was 38 mm. Considering the speed of sound at room temperature in water based agar gelatin phantoms, the wavelength of ultrasound was around 0.33 mm. The probe had two modes : one to transmit and one to image. In the transmitting mode, a sequence of three pushes at the depths of 25, 30 and 35 mm from the surface of the phantoms, with a time delay from each other, produced a cone beam and the shear wave propagated in the medium. The pushing time was 125 μs. The ultra

fast imaging (plane wave imaging) method was used as the imaging mode with a high frame rate of 4000 frames per second. The depth of imaging was 64 mm. Each acquisition was repeated 5 times. The RF signals were stored on a work station.

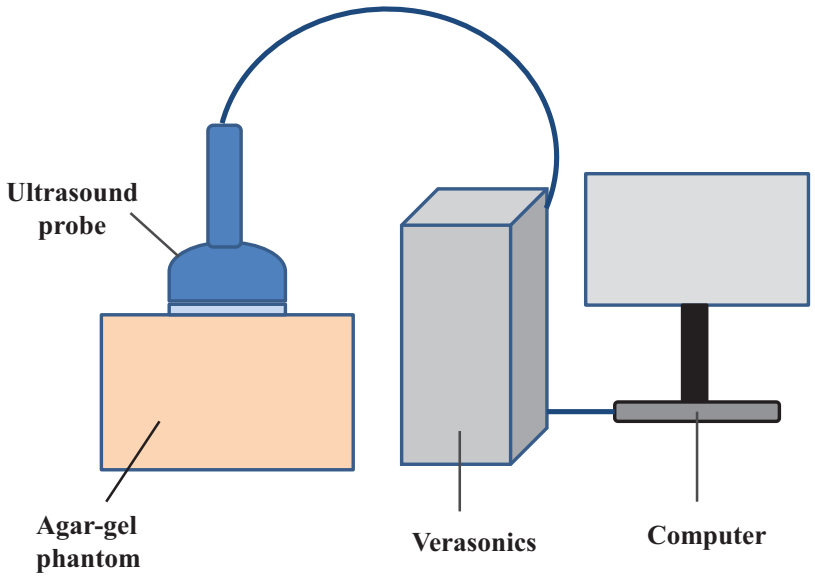

FIGURE 3.4 – Schematic diagram of the experimental set-up.

Moreover, the elasticity of the homogenous phantoms were measured by the Aixplorer system (Supersonic Imagine, France). Figure 3.5 shows the device that provided the elasticity map, the B-mode images, and the estimates of the Young's modulus.

FIGURE 3.5 – Aixplorer system.

3.4.2 *Ex-vivo* measurements

The *ex-vivo* set-up was similar to Figure 3.4 with a heterogeneous phantom instead (an agar gelatin phantom with a mouse tumor as inclusion). The radiation force was applied at the center of the phantom, while the tumor was placed on one side of the phantom.

3.5 Data processing

The data was obtained and processed with and without shear wave propagation. The next step was the RF data analysis during shear wave propagation. Data analysis in both sets of experiments (*in-vitro* and *ex-vivo*) was quite similar.

Data post processing of the *in-vitro* and *ex-vivo* experiments is explained in this section. The region of interest (ROI) for both sets of experiments is defined and the analysis procedure is explained. The estimator of the homodyned K-distribution is presented.

3.5.1 The choice of the ROI

To estimate the parameters of the homodyned K-distribution with and without shear wave propagation, a specific region (ROI) on the B-mode images was defined. The choice of the ROI for the *in-vitro* and *ex-vivo* experiments is discussed in the following subsections.

3.5.1.1 *In-vitro* ROI

The ROI for the *in-vitro* experiments was a square with a width and length of 10 mm. Figure 3.6 shows the position of the ROI, which is 5 mm far from the first focal spot of the applied radiation force. The rationale behind the choice of the ROI is to have a region far enough from the pushing beam to avoid noisy curves of the statistical parameters during shear wave propagation and without being too far to avoid a poor signal quality due to shear wave attenuation. The depth of the ROI was chosen around the depth of the first focal spot. The size of the ROI is justified by considering the typical size of the mouse tumors in the *ex-vivo* experiments. It is consistent with the recommended minimal ROI size of three times the wavelength (26).

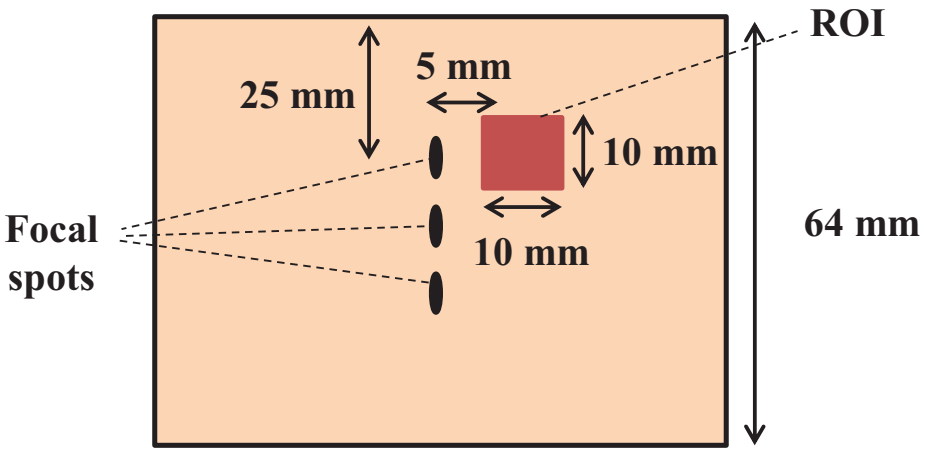

FIGURE 3.6 – ROI in *in-vitro* experiments.

3.5.1.2 *Ex-vivo* ROI

For the *ex-vivo* experiments, the goal was to study the effect of shear wave propagation inside the tumor and to discriminate the tumors from their surrounding medium. Therefore, two ROIs

were defined with the same size and the same distance from the pushing beams, one for the tumor and the other one for the surrounding medium on the other side of the pushing beams. The ROIs were chosen as follows : 1) the ROI enclosed by the manually segmented contours of the mice tumors ; 2) the ROI in the surrounding medium, symmetric to the tumor ROI with respect to the vertical axis along the focal spots of the pushing beam (Figure 3.7).

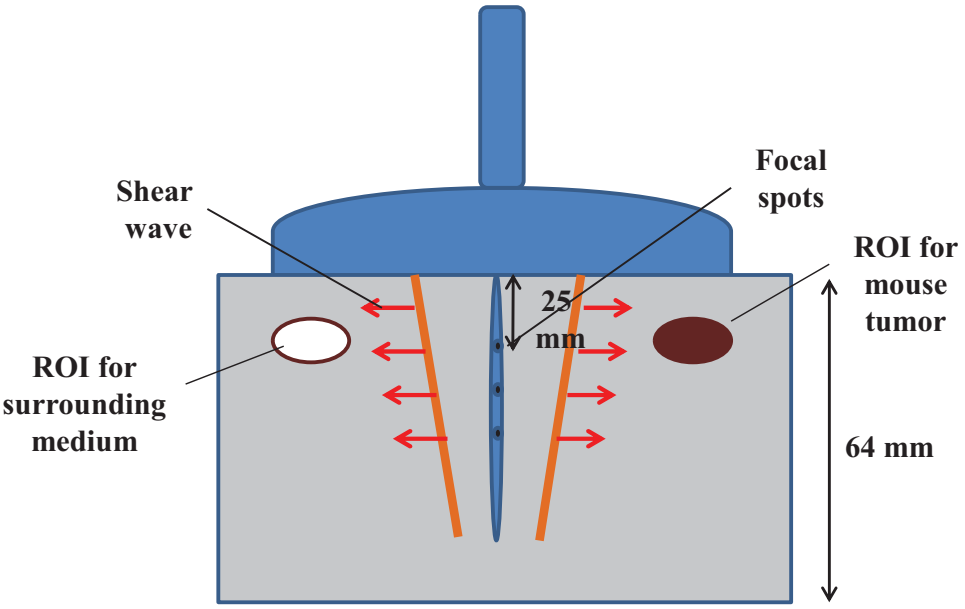

FIGURE 3.7 – ROI in *ex-vivo* experiments.

3.5.1.3 *In-vitro* data processing

Figure 3.8 shows the *in-vitro* data processing diagram. The *f-k* migration algorithm was applied on the experimental RF data (20). To reconstruct the B-mode images, the Hilbert transform (30) was used to process RF data without any logarithmic compression. The parameters of the homodyned K-distribution were estimated over the ROI (14). The displacement map of the medium during shear wave propagation was also extracted from the RF data, using the GPU implementation of the cross-correlation algorithm (41).

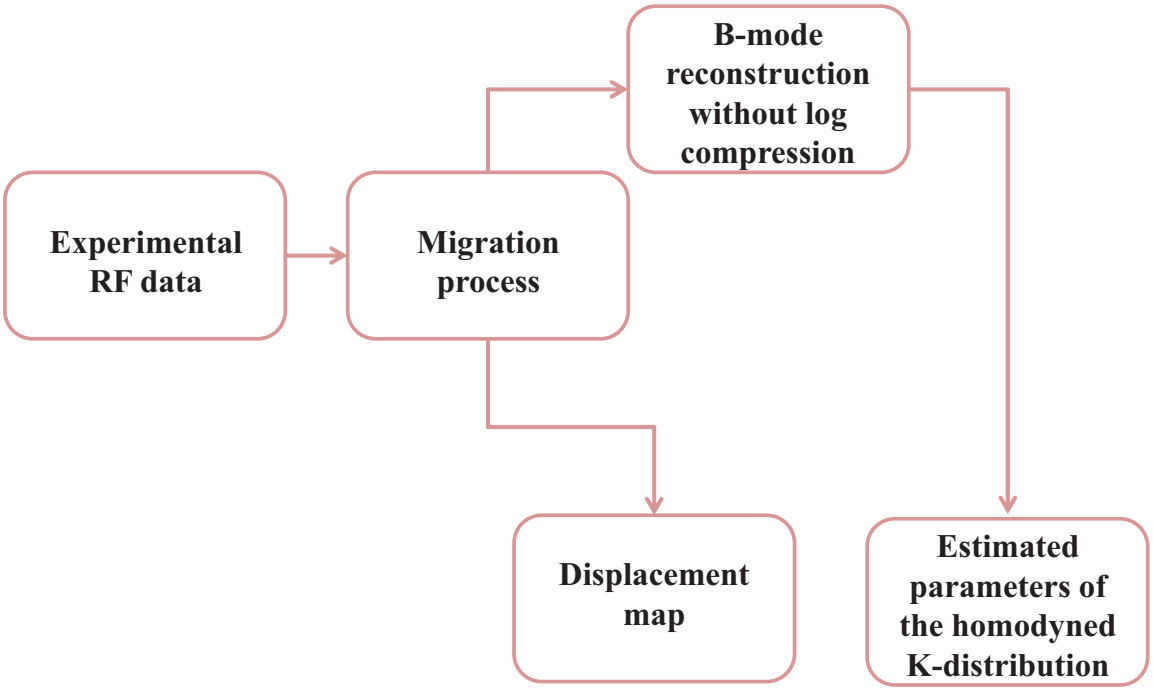

FIGURE 3.8 – *In-vitro* data processing diagram.

3.5.1.4 *Ex-vivo* data processing

Figure 3.9 presents the *ex-vivo* data processing diagram. In this part, the last two hypotheses were examined. To compare the behavior of the parameters of the homodyned K-distribution under shear wave propagation inside and outside the tumor, two regions were defined in each heterogeneous phantom as explained above. To visualize the tumor on the B-mode images, log compression was used after applying the Hilbert transform of the RF lines. The homodyned K-distribution estimator was applied on the B-mode images without log compression.

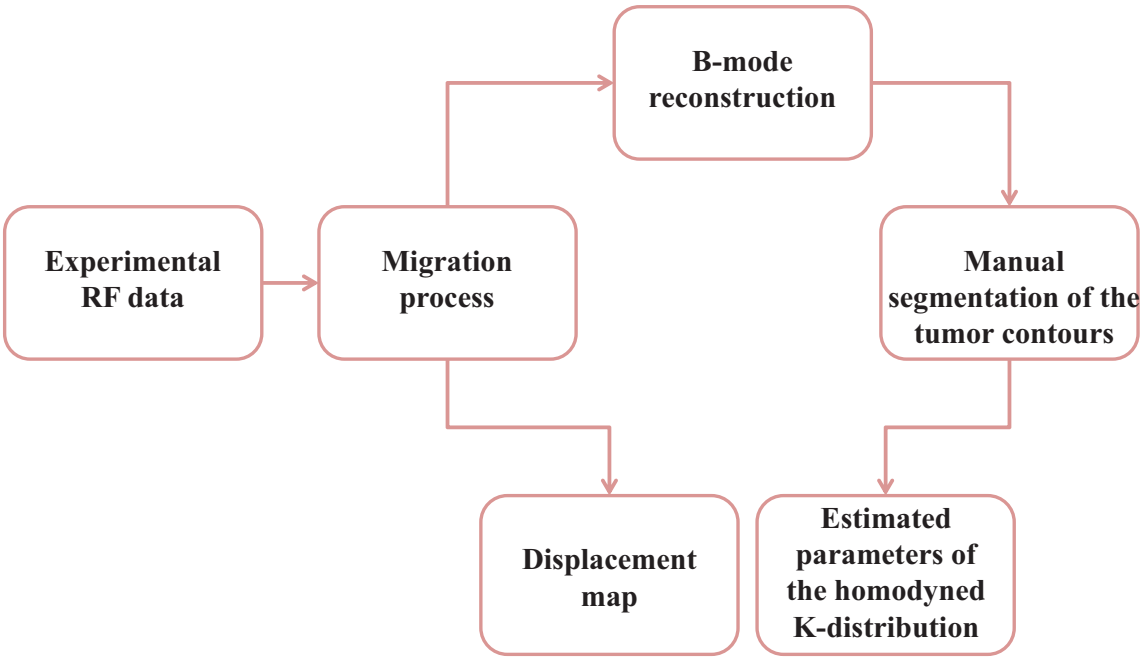

FIGURE 3.9 – *Ex-vivo* data processing diagram.

3.5.2 Homodyned K-distribution estimator

The α parameter and the κ parameter of the homodyned K-distribution are invariant to the mean intensity (14). In this work, the three parameters that were studied with and without shear wave propagation are presented in Table 3.III.

TABLE 3.III – Three estimated parameters of the homodyned K-distribution.

Parameter	Physical interpretation
α	scatterer clustering parameter
$\kappa = \frac{\varepsilon^2}{2\sigma^2\alpha}$	structure parameter
$\mu = \varepsilon^2 + 2\sigma^2\alpha$	mean intensity (total signal power)

The parameters of the homodyned K-distribution were estimated based on the mean intensity and and two log-moments with the method developed in (14).

CHAPITRE 4

RESULTS

In this chapter, the results from the *in-vitro* and *ex-vivo* experiments are presented. The experimental data processing to achieve the time evolution of the homodyned K-distribution parameters during shear wave propagation with the SSI method is presented. The preliminary results that are presented in appendices I and II, i.e. the two published proceedings, are summarized briefly in the first section. The remaining part of this chapter presents the results of the two sets of experiments (*in-vitro* and *ex-vivo*) corresponding to the five hypotheses.

4.1 Preliminary results found in appendices

Our first observations in dynamic QUS were *in-vitro* experiments with agar gelatin phantoms. Plane shear waves were generated by an external vibrator and a rigid plate. The K-distribution was considered as ultrasound echo envelope statistical model. The K-distribution corresponds to the special case of the homodyned K-distribution in the absence of a coherent signal component.

The preliminary results showed that the shear wave propagation could be tracked by the time evolution of the reciprocal of the α parameter of the K-distribution. The parameter $1/\alpha$ had a similar pattern as the displacement map at the central point of the homogenous agar gelatin phantoms (see appendix I). To avoid the case $\alpha = \infty$, which is meaningless, the reciprocal of the parameter α was proposed in (17), (13).

The second step was to consider a heterogeneous medium and to assess if dynamic QUS could provide extra information to differentiate between an inclusion and its surrounding medium (see appendix II). An agar gelatin phantom with two agar gelatin inclusions with different mechanical properties was fabricated. The parameter $1/\alpha$ was estimated for the surrounding medium and both inclusions, with and without shear wave propagation. The results showed that the static value of $1/\alpha$ could barely distinguish one of the inclusions from the surrounding medium ; however, the dynamic range of the $1/\alpha$ parameter succeeded in this task for both inclusions. These preliminary results were a motivation to consider dynamic QUS features in the context of tissue characterization.

4.2 *In-vitro* results

Following the phantom fabrication method presented in the previous chapter, three homogenous phantoms (*A*, *B*, *C*) were made. A shear wave was propagated from the center of the phantoms using the SSI method. The displacement map was estimated with the normalized cross-correlation method. Figure 4.1 shows the maximum spatial displacement map of the medium in phantom *B*. The cone-shaped shear wave front can be seen in this figure.

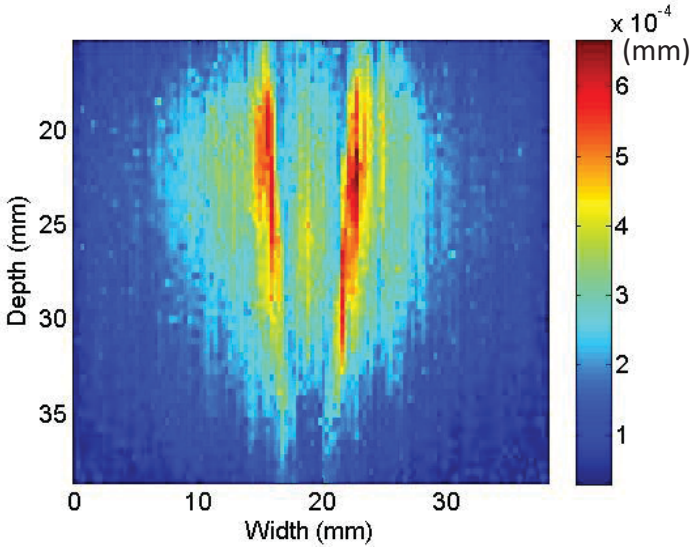

FIGURE 4.1 – Maximum displacement map of the medium in phantom *B*.

In the following sections, the results corresponding to each hypothesis are presented.

4.2.1 Hypothesis 1

Hypothesis 1 : The parameters of the homodyned K-distribution from ultrasound echo envelope data are affected by shear wave propagation.

According to the first hypothesis, shear wave propagation affects the homodyned K-distribution parameters estimated from ultrasound echo envelope data. The parameters of the homodyned K-

distribution were estimated in the chosen ROI with the data processing method described in chapter 3.

Figure 4.2 shows the point wise displacement of the central point in the ROI for phantom *B*. Since the radiation pressure push impulse was applied at the 6th frame, the first five frames were considered as being in the static mode. The shear wave propagation occurred from the 7th frame to the 100th frame. As expected with the SSI method, the displacement was attenuated rapidly over time.

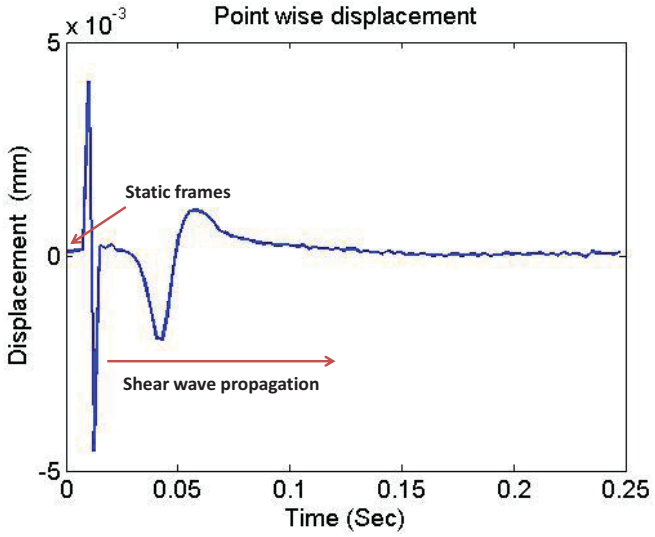

FIGURE 4.2 – Point wise displacement at the central point of the ROI of phantom *B*.

The effect of the shear wave propagation on the homodyned K-distribution parameters can be seen in Figures 4.3, 4.4 and 4.5. As one can see, the largest change in the homodyned K-parameters occurred at the same frame as one of the two main glitches in the displacement curve of Figure 4.2, which corresponds to the time of the push impulse. Figure 4.3 shows the time evolution of the α parameter during shear wave propagation. As mentioned before, the α parameter is interpreted as a scatterer clustering parameter. To evaluate the hypotheses, the parameter α was chosen instead of $1/\alpha$ (as seen in preliminary results), because the case $\alpha = \infty$ did not occur and it was easier to see the evolution of α than $1/\alpha$ in the present results.

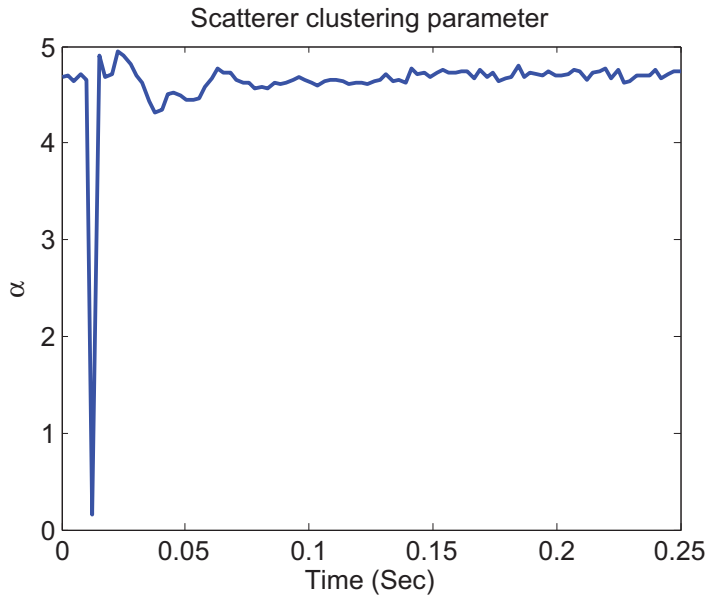

FIGURE 4.3 – Time evolution of the α parameter over the ROI of phantom *B*.

Figure 4.4 presents the dynamic behavior of the structure parameter (the κ parameter). The mean intensity of the ultrasound echo envelope (the μ parameter) during shear wave propagation is presented in Figure 4.5.

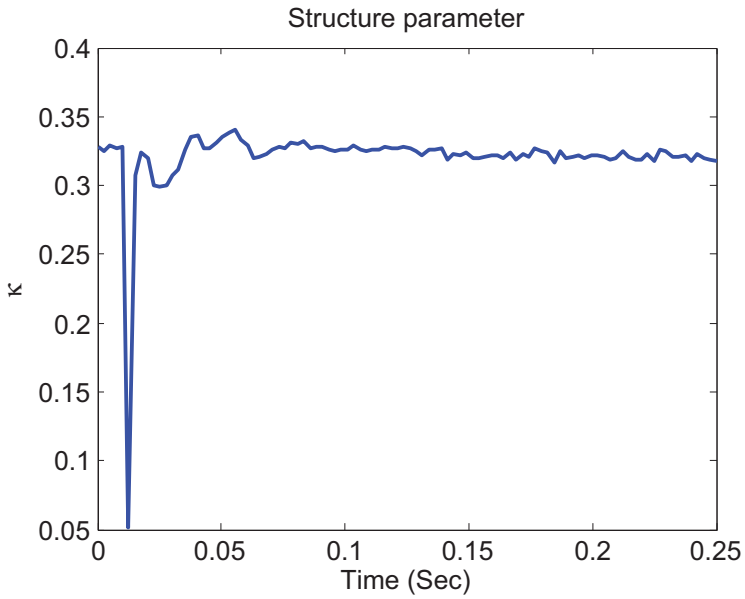

FIGURE 4.4 – Time evolution of the κ parameter over the ROI of phantom *B*.

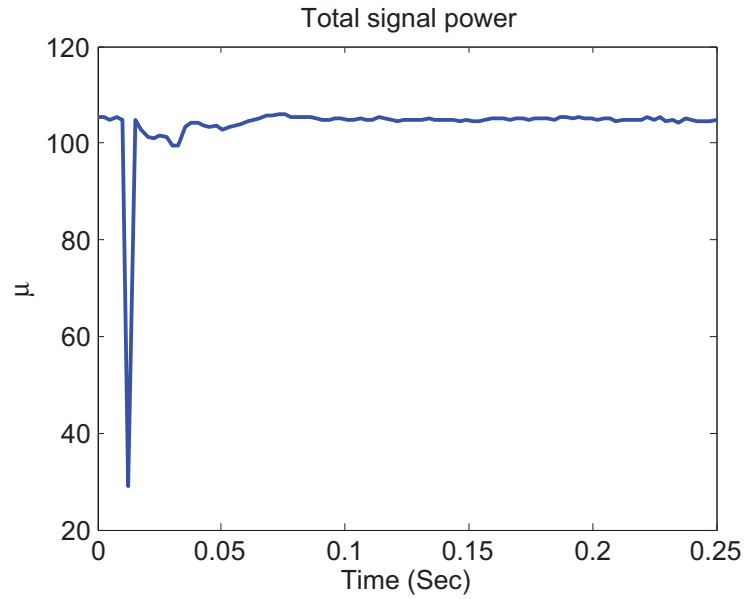

FIGURE 4.5 – Time evolution of the μ parameter over the ROI of phantom *B*.

For quantitative analysis, the range of the parameters of the homodyned K-distribution during shear wave propagation were considered. The range of a parameter a is defined as the difference between the maximal and minimal values of the parameter over the sequence of temporal images : Range(a) = Max(a)- Min(a).

Note that the goal of this hypothesis was to show that the shear wave propagation affects significantly the homodyned K-distribution parameters. In order to verify this hypothesis, the ranges of the statistical parameters under shear wave propagation were compared with the ranges of the same parameters without shear wave propagation. This comparison was only assessed for hypothesis 1 and should not be confused with comparisons between dynamic and static QUS that were assessed for the remaining hypotheses. In the latter case, as explained in section 3.1, the range of the parameters is used in the context of dynamic QUS, whereas the median (or mean value) is considered in the context of static QUS. For the *in-vitro* experiments, the static range of each statistical parameter was estimated by considering the first five frames, and the dynamic range was calculated from the 7th frame to the 100th. Considering five acquisitions over a given phantom, the mean and standard deviation of each parameter were estimated. Table 4.I presents the static and dynamic ranges of the homodyned K-distribution parameters. The indexes s and d represent static and dynamic values, respectively. As one can see, the ranges of the parameters under shear wave propagation were substantially larger than the ranges of the same parameters without shear wave propagation, except for the parameter κ in the case of phantom C.

TABLE 4.I – Static and dynamic ranges of the parameters of the homodyned K-distribution for the three homogenous phantoms.

	A	B	C
$Range(\alpha_s)$	0.77±0.25	0.05±0.02	0.12±0.09
$Range(\kappa_s)$	0.02±0.003	0.003±0.001	0.00±0.00
$Range(\mu_s)$	0.95±0.31	0.42±0.10	0.41±0.11
$Range(\alpha_d)$	8.34±2.03	0.69±0.06	0.56±0.01
$Range(\kappa_d)$	0.12±0.02	0.05±0.004	0.00±0.00
$Range(\mu_d)$	18.31±0.74	6.09±0.26	2.65±0.16

Table 4.II presents the results of two-way ANOVA tests to evaluate the effect of the shear

wave propagation on the parameters of the homodyned K-distribution. The results show that there is a statistically significant difference between the static and dynamic ranges of the homodyned K-distribution parameters except for the κ parameter of phantom *C*. Here, a two-way ANOVA test was applied with two factors : 1) static versus dynamic range of homodyned K-distribution parameters ; and 2) labels of phantoms (*A*, *B*, *C*). Note that the κ parameter for phantom *C* was zero for all frames except at the 6th frame, as presented in Table 4.I. This may be related to the stiffness of the phantom. Phantom C has the largest stiffness and the smallest displacement amplitude among the three *in-vitro* phantoms. As observed, the κ parameter of phantom *C* was not affected by a small displacement amplitude. Based on these results, hypothesis 1 was overall verified.

TABLE 4.II – Two-way ANOVA tests to compare static and dynamic ranges of each parameter of the homodyned K-distribution for phantoms A, B and C. (* : The κ parameter for phantom C was zero in all frames except during the push impulse.)

$Two-way\ ANOVA$ ($p < 0.001$)	*A*	*B*	*C*	*Overall*
$Range(\alpha_d)\ vs.\ Range(\alpha_s)$	yes	yes	yes	yes
$Range(\kappa_d)\ vs.\ Range(\kappa_s)$	yes	yes	no*	yes
$Range(\mu_d)\ vs.\ Range(\mu_s)$	yes	yes	yes	yes

The coefficient of variation (*CV*) is defined as the ratio of the standard deviation to the mean value of a series of variables. Table 4.III shows the coefficients of variation of static and dynamic ranges of homodyned K-distribution parameters over five acquisitions. Note that "NA" means not applicable in the case of κ, since its mean and standard deviation are equal to zero.

TABLE 4.III – Coefficients of variation (CV) of static and dynamic ranges of homodyned K-distribution parameters for phantoms A, B and C.

	A	B	C
$CV(Range(\alpha_s))$	0.32	0.40	0.75
$CV(Range(\kappa_s))$	0.15	0.33	NA
$CV(Range(\mu_s))$	0.30	0.24	0.27
$CV(Range(\alpha_d))$	0.24	0.084	0.014
$CV(Range(\kappa_d))$	0.15	0.083	NA
$CV(Range(\mu_d))$	0.041	0.042	0.062

4.2.2 Hypothesis 2

Hypothesis 2 : The range of the parameters of the homodyned K-distribution during shear wave propagation can be used to discriminate different tissue mimicking phantoms.

The second hypothesis is related to the ability of static and dynamic QUS to differentiate between the tissue mimicking phantoms. As discussed in section 3.1, to estimate the statistical parameters in the context of static QUS, the median of the homodyned K-distribution parameters in static mode were computed for each acquisition. These parameters are expected to depend on the microstructure properties of the medium. For dynamic QUS, the ranges of the homodyned K-distribution parameters were computed and are expected to be related mainly to mechanical properties of the medium. Their mean and standard deviation were obtained by considering five acquisitions (Table 4.IV). As one can see, overall, the various parameters are different for the three phantoms, taking into account their mean values and standard deviations.

TABLE 4.IV – Static values and dynamic ranges of the homodyned K-distribution parameters for phantoms A, B and C.

	A	*B*	*C*
α_s	12.91±0.12	4.63±0.10	18.11±0.10
κ_s	0.29±0.003	0.33±0.006	0.00±0.00
μ_s	133.61±0.44	104.75±0.64	131.00±0.15
$Range(\alpha_d)$	8.34±2.03	0.69±0.06	0.56±0.01
$Range(\kappa_d)$	0.12±0.02	0.05±0.004	0.00±0.00
$Range(\mu_d)$	18.31±0.74	6.09±0.26	2.65±0.16

Table 4.V presents the results of two-way ANOVA tests to examine the ability of the static values and dynamic ranges of the three parameters of the homodyned K-distribution to distinguish between each pair of phantoms. Note that the dynamic ranges of the α parameter of phantoms *B* and *C* did not overlap (Table 4.IV). However, these two phantoms were not distinguished using the two-way ANOVA test when the ANOVA test was applied on the three phantoms together. Indeed, the dynamic range of the α parameter of phantom *A* was one order of magnitude greater than for the other two phantoms. When we removed phantom *A* from the ANOVA test, phantoms *B* and *C* were distinguished by the dynamic range of the α parameter.

TABLE 4.V – Two-way ANOVA test results to evaluate the discrimination ability of the static values and dynamic ranges of the homodyned K-distribution parameters. (* : Note that here, two-way ANOVA tests were performed on the three phantoms, while the range of the α parameter could distinguish between phantoms *B* from *C* when phantom *A* is not considered.)

$Two-way\ ANOVA$ (p < 0.001)	*AB*	*AC*	*BC*
α_s	yes	yes	yes
κ_s	yes	yes	yes
μ_s	yes	yes	yes
$Range(\alpha_d)$	yes	yes	no* (p=0.968)
$Range(\kappa_d)$	yes	yes	yes
$Range(\mu_d)$	yes	yes	yes

Table 4.VI shows the coefficients of variation of static values and dynamic ranges of homodyned K-distribution parameters over five acquisitions. Note that "NA" means not applicable in the case of κ, since its mean and standard deviation vanish.

TABLE 4.VI – Coefficients of variation of static values and dynamic ranges of homodyned K-distribution parameters for phantoms A, B and C.

	A	*B*	*C*
$CV(\alpha_s)$	0.0093	0.022	0.0054
$CV(\kappa_s)$	0.0085	0.017	NA
$CV(\mu_s)$	0.0033	0.0061	0.0012
$CV(Range(\alpha_d))$	0.24	0.084	0.014
$CV(Range(\kappa_d))$	0.15	0.083	NA
$CV(Range(\mu_d))$	0.041	0.042	0.062

4.2.3 Hypothesis 3

Hypothesis 3 : The maximal displacement amplitude of the medium and the reciprocal of the Young's modulus are correlated with the range of the parameters of the homodyned K-distribution during shear wave propagation.

The third hypothesis is based on a linear regression between the range of the homodyned K-distribution parameters during shear wave propagation and the mechanical properties of the medium. Table 4.VII, recalls from Table 4.IV the dynamic range of the parameters of the homodyned K-distribution, and presents the Young's modulus (E) and the maximal displacement amplitude at the central point of the defined ROI for the three phantoms. Note that based on the Young's modulus values E, phantoms A, B and C are in order of increasing stiffness (i.e., increasing values of E) and henceforth, in order of decreasing maximal displacement amplitude.

TABLE 4.VII – The dynamic range of the homodyned K-distribution parameters, Young's modulus and the maximal displacement amplitude of each phantom.

	A	B	C
$Range(\alpha_d)$	8.34±2.03	0.69±0.06	0.56±0.01
$Range(\kappa_d)$	0.12±0.02	0.05±0.004	0.00±0.00
$Range(\mu_d)$	18.31±0.74	6.09±0.26	2.65±0.16
$E(kPa)$	17.52	21.76	44.05
Maximum displacement amplitude (μm)	4.0 ±3.84e-004	1.7 ±0.001	0.6 ±9.9835e-005

A regression test based on the values in Table 4.VII was performed considering a linear regression, $Y = aX + b$, between the static values or the dynamic range of the homodyned K-distribution parameters, X, and the maximal displacement amplitude or the $1/E$ parameter, Y. The $1/E$ parameter was chosen instead of E because we expected that a smaller displacement amplitude (and a smaller range of the homodyned K-distribution parameters) would correspond to a larger value of the Young's modulus (i.e., a greater stiffness). The R^2 coefficients of determi-

nation, the parameters a and b, and the p values are presented in Tables 4.VIII (linear regression with maximum amplitude displacement) and 4.IX (linear regression with $1/E$).

As seen from these tables, the R^2 coefficients of determination between the dynamic range of homodyned K-distribution parameters and the maximum displacement amplitude were greater than 0.84 (with $p < 0.001$). The maximum R^2 coefficient of determination was obtained for the case of the dynamic range of the μ parameter and the maximum displacement amplitude with a value of 0.98 and $p < 0.001$. On the other hand, the linear regression between the static values of the homodyned K-distribution parameters and the maximum displacement amplitude were relatively low (Table 4.VIII). Dynamic QUS parameters were correlated with the $1/E$ parameter with a maximum R^2 value of 0.87 obtained for the κ parameter (with $p < 0.001$). The R^2 coefficient of determination between the dynamic range of the μ parameter and $1/E$ was 0.76 (with $p < 0.001$). For the static QUS parameters, the α and μ parameters were not correlated with $1/E$, but the static κ parameter was correlated with $1/E$ with an R^2 coefficient of determination of 0.82 (with $p < 0.001$).

TABLE 4.VIII – The R^2 coefficient of determination, a and b parameters and the p values from the linear regression tests of the static values or the dynamic ranges of the homodyned K-distribution parameters and the maximal displacement amplitudes for the *in-vitro* phantoms.

(α_s)	(κ_s)	(μ_s)
$R^2 = 0.04$ $a = 0.027, b = 0.000$ $p = 0.474$	$R^2 = 0.46$ $a = 0.008, b = 0.067$ $p = 0.005$	$R^2 = 0.07$ $a = 0.015, b = 0.000$ $p = 0.328$
$Range(\alpha_d)$	$Range(\kappa_d)$	$Range(\mu_d)$
$R^2 = 0.84$ $a = 0.010, b = 0.003$ $p < 0.001$	$R^2 = 0.96$ $a = 0.006, b = 0.281$ $p < 0.001$	$R^2 = 0.98$ $a = 0.002, b = 0.002$ $p < 0.001$

TABLE 4.IX – The R^2 coefficient of determination, a and b parameters and the p values from the linear regression tests of the static values and the dynamic ranges of the homodyned K-distribution parameters and the parameter $1/E$ for the *in-vitro* phantoms.

(α_s)	(κ_s)	(μ_s)
$R^2 = 0.31$	$R^2 = 0.82$	$R^2 = 0.15$
$a = 0.059, b = 0.001$	$a = 0.024, b = 0.088$	$a = 15.022, b = 0.195$
p = 0.474	p < 0.001	p = 0.160
$Range(\alpha_d)$	$Range(\kappa_d)$	$Range(\mu_d)$
$R^2 = 0.53$	$R^2 = 0.87$	$R^2 = 0.76$
$a = 0.033, b = 0.003$	$a = 0.027, b = 0.263$	$a = 0.0254, b = 0.002$
p = 0.002	p < 0.001	p < 0.001

4.3 *Ex-vivo* results

This section presents the results of the *ex-vivo* phantoms with a mouse tumor as an inclusion. For the heterogeneous phantoms, T_I and T_{II}, S_I and S_{II} indicate the first and second tumors and the corresponding surrounding media, respectively.

Figure 4.6 shows a B-mode image of phantom II. To define the tumor region, its contours were manually segmented in the B-mode images. The segmentation of the tumor region was helped by its known position from the experimental set up and the shadow effect below the tumor due to ultrasound attenuation. To specify the surrounding medium, the determined tumor region was reflected with respect to the vertical axis along the focal spots (Figure 4.7). Therefore, the surrounding medium and the tumor areas had the same size and the same distance from the focal spots of the radiation force. Figures 4.8 and 4.9 show the point wise displacement map inside the two tumors. In the *ex-vivo* experiments, the shear wave was propagated from the second frame to the 100th frame. The static frames were considered as the last five frames where the displacement amplitude was approximately zero (Figure 4.8).

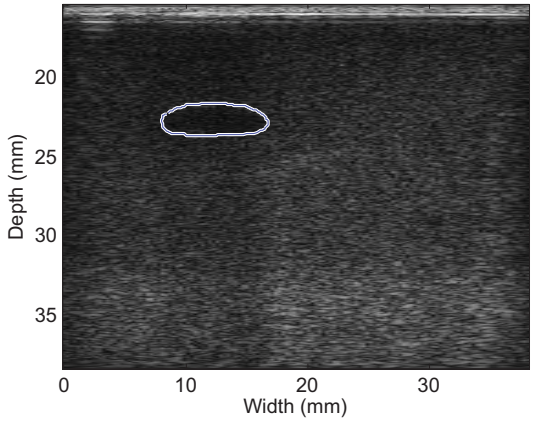

FIGURE 4.6 – The B-mode image of phantom *II* and the segmented tumor region.

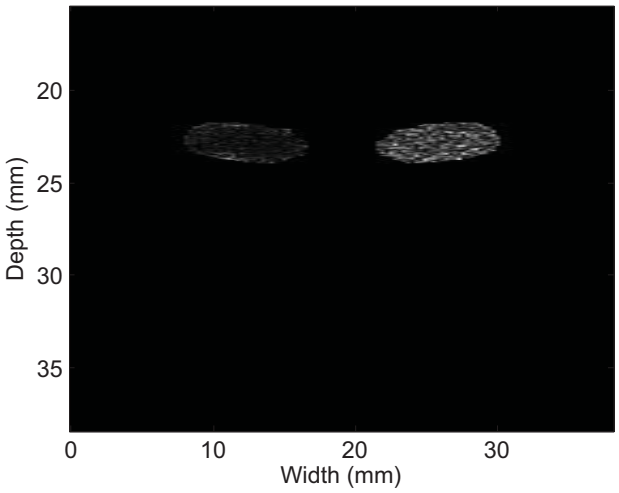

FIGURE 4.7 – The mask of the segmented tumor and its reflected region as the corresponding surrounding medium in phantom *II*.

Figures 4.10 to 4.15 show the time evolution of the homodyned K-distribution parameters estimated on the segmented tumors. As one can see, the largest change in the parameters occurred at the same frame as one of the glitches in the displacement amplitude curve. The shear wave

propagation was considered as occurring in the subsequent frames.

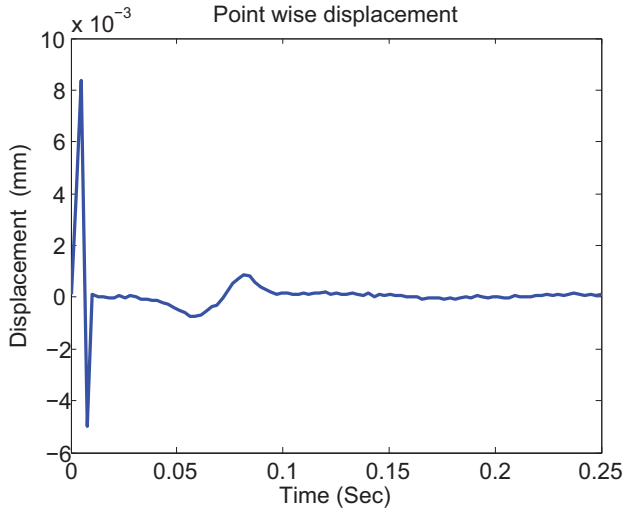

FIGURE 4.8 – Point wise displacement of the central point of tumor T_I during shear wave propagation.

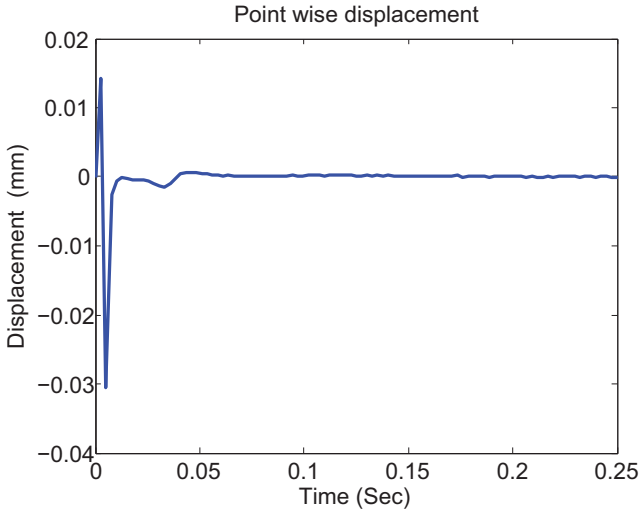

FIGURE 4.9 – Point wise displacement of the central point of tumor T_{II} during shear wave propagation.

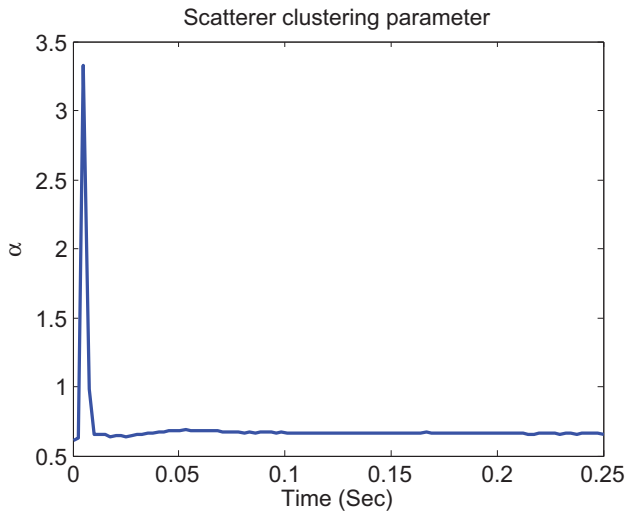

FIGURE 4.10 – Time evolution of the α parameter of the homodyned K-distribution of tumor T_I.

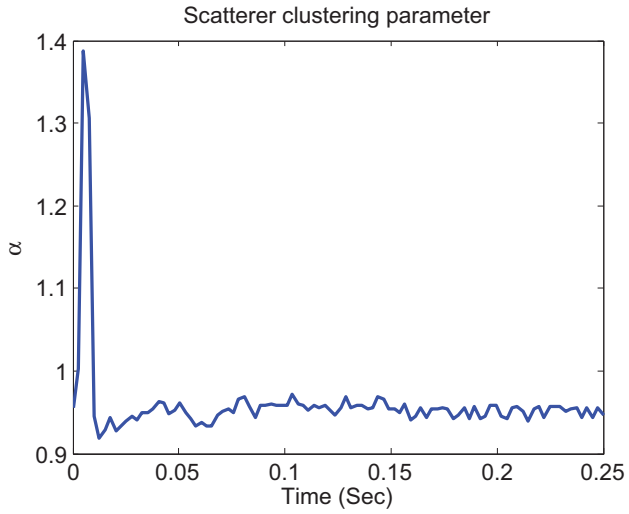

FIGURE 4.11 – Time evolution of the α parameter of the homodyned K-distribution of tumor T_{II}.

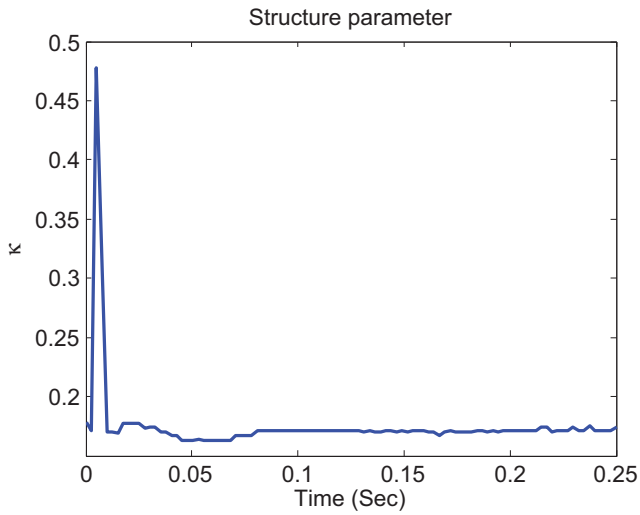

FIGURE 4.12 – Time evolution of the κ parameter of the homodyned K-distribution of tumor T_I.

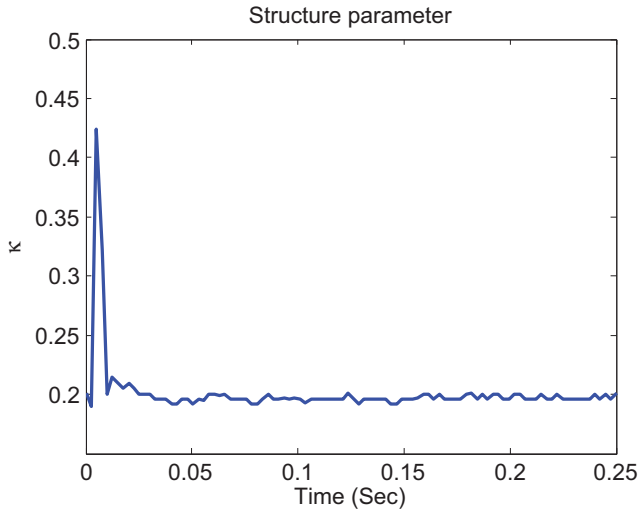

FIGURE 4.13 – Time evolution of the κ parameter of the homodyned K-distribution of tumor T_{II}.

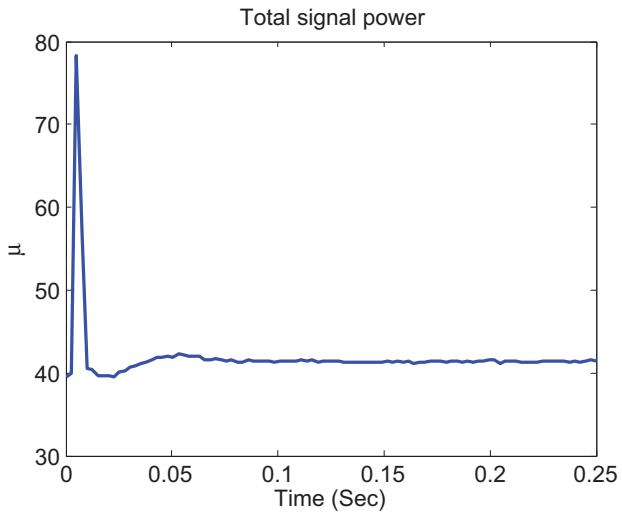

FIGURE 4.14 – Time evolution of the μ parameter of the homodyned K-distribution of tumor T_I.

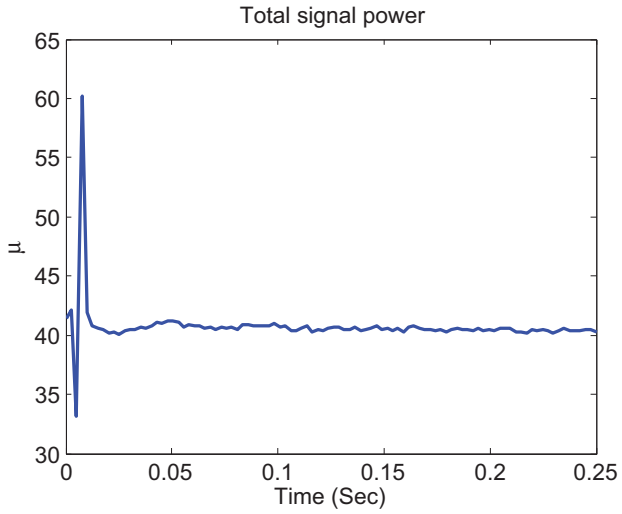

FIGURE 4.15 – Time evolution of the μ parameter of the homodyned K-distribution of tumor T_{II}.

4.3.1 Hypothesis 4

Hypothesis 4 : Dynamic QUS can help in distinguishing the mice tumors from their surrounding medium.

The goal of this section was to study the ability of dynamic QUS to differentiate between tumors and their surrounding medium. Table 4.X presents the static values and the dynamic ranges of the homodyned K-distribution parameters for the two tumors and their surrounding medium. As one can see, overall, the various parameters are different for the tumors and their surrounding media, taking into account their mean values and standard deviations.

TABLE 4.X – The static values and the dynamic ranges of the homodyned K-distribution parameters for the two tumors and their surrounding medium.

	T_I	S_I	T_{II}	S_{II}
α_s	0.67 ± 0.007	21.95±0.316	0.94± 0.007	9.30±0.12
κ_s	0.17±0.002	0.00 ±0.00	0.20±0.003	0.42± 0.005
μ_s	42.00±0.57	130.19±0.15	40.17±0.18	99.84±0.34
$Range(\alpha_d)$	0.04±0.004	6.60±0.06	0.04±0.00005	3.31±0.86
$Range(\kappa_d)$	0.01 ± 0.001	0.00 ± 0.00	0.02±0.0003	0.07 ±0.014
$Range(\mu_d)$	2.94± 0.13	7.20±0.18	1.24±0.19	3.26± 0.18

Table 4.XI presents the results of two-way ANOVA tests to assess the ability of the static values and dynamic ranges of the three parameters of the homodyned K-distribution to differentiate between the tumors and their surrounding media. Based on these results, hypothesis 4 is confirmed.

TABLE 4.XI – The results of two-way ANOVA test to evaluate the ability of the static value and dynamic range of the homodyned K-distribution parameters to differentiate tumors from their surrounding medium.

$Two-way\ ANOVA$ ($p < 0.001$)	$T_I - S_I$	$T_{II} - S_{II}$
α_s	yes	yes
κ_s	yes	yes
μ_s	yes	yes
$Range(\alpha_d)$	yes	yes
$Range(\kappa_d)$	yes	yes
$Range(\mu_d)$	yes	yes

Table 4.XII presents, as extra information, the results of two-way ANOVA tests to see if there were significant differences in the various parameters between the two tumors, and also between the two surrounding media. The results show that half of the parameters distinguish the two tumors, whereas all parameters differentiate the two surrounding media.

TABLE 4.XII – The results of two-way ANOVA test to see if there were significant differences in the various parameters between the two tumors, and also between the two surrounding media.

$Two-way\ ANOVA$	$T_I - T_{II}$	$S_I - S_{II}$
α_s	no, $p = 0.828$	yes, $p < 0.001$
κ_s	yes, $p < 0.001$	yes, $p < 0.001$
μ_s	yes, $p = 0.003$	yes, $p < 0.001$
$Range(\alpha_d)$	no, $p = 1.000$	yes, $p < 0.001$
$Range(\kappa_d)$	no, $p = 0.578$	yes, $p < 0.001$
$Range(\mu_d)$	yes, $p = 0.003$	yes, $p < 0.001$

4.3.2 Hypothesis 5

Hypothesis 5 : The maximal displacement amplitude of the mice tumors is correlated with the range of the parameters of the homodyned K-distribution during shear wave propagation.

The last hypothesis is based on a linear regression between the range of the homodyned K-distribution parameters during shear wave propagation and the maximal displacement amplitude of the medium in the tumors. Note that hypothesis 3 was assessed with the three *in-vitro* phantoms, whereas hypothesis 5 was assessed in the context of the *ex-vivo* experiments. Moreover, in the context of the *ex-vivo* experiments, the Young's modulus measurements were unfortunately not available, so that only the maximal displacement amplitude was used in the analysis. A regression test was performed considering a linear regression, $Y = aX + b$, between the static values or the dynamic range of the homodyned K-distribution parameters, X, and the maximal displacement amplitude Y for the mice tumors and their surrounding medium, respectively. The R^2 coefficients of determination, the parameters a and b and the p values for the tumors and their surrounding medium are presented in Tables 4.XIII and 4.XIV, respectively.

According to Tables 4.XIII and 4.XIV, the dynamic range of the μ parameter yielded a greater R^2 coefficient of determination in comparison to the other parameters, for both of the tumors and their surrounding medium with an R^2 = 0.56 (with p = 0.013) and R^2 = 0.59 (with p = 0.009), respectively. The maximum R^2 coefficient of determination between the maximum displacement amplitude and the static values of the homodyned K-distribution parameters was observed for the μ parameter of the tumors and their surrounding medium with an R^2 = 0.55 (with p = 0.022) and R^2 = 0.45 (with p = 0.047) , respectively.

TABLE 4.XIII – The R^2 coefficients of determination, a and b parameters and the p values of the linear regression tests of the static values and the dynamic ranges of the homodyned K-distribution parameters and the maximal displacement amplitudes of the tumors of the *ex-vivo* phantoms.

(α_s)	(κ_s)	(μ_s)
$R^2 = 0.48$ $a = 0.796, b = 0.734$ p = 0.038	$R^2 = 0.48$ $a = 1.339, b = 6.135$ p = 0.038	$R^2 = 0.55$ $a = 4.134, b = 0.106$ p = 0.022
$Range(\alpha_d)$	$Range(\kappa_d)$	$Range(\mu_d)$
$R^2 = 0.002$ $a = 0.112, b = 2.219$ p = 0.088	$R^2 = 0.32$ $a = 0.766, b = 33.270$ p = 0.088	$R^2 = 0.56$ $a = 0.046, b = 0.120$ p = 0.013

TABLE 4.XIV – The R^2 coefficients of determination, a and b parameters and the p values of the linear regression tests of the static values and the dynamic ranges of the homodyned K-distribution parameters and the maximal displacement amplitudes of the surrounding medium of the *ex-vivo* phantoms.

(α_s)	(κ_s)	(μ_s)
$R^2 = 0.43$ $a = 0.066, b = 0.014$ p = 0.056	$R^2 = 0.44$ $a = 0.242, b = 0.430$ p = 0.050	$R^2 = 0.45$ $a = 0.534, b = 0.006$ p = 0.047
$Range(\alpha_d)$	$Range(\kappa_d)$	$Range(\mu_d)$
$R^2 = 0.51$ $a = 0.140, b = 0.063$ p = 0.021	$R^2 = 0.54$ $a = -0.612, b = 9.546$ p = 0.016	$R^2 = 0.59$ $a = 0.113, b = 0.049$ p = 0.009

CHAPITRE 5

DISCUSSION AND CONCLUSION

5.1 Discussion of the results

The aim of this study is to propose a new method in QUS by considering the range of the homodyned K-distribution parameters during shear wave propagation, in order to obtain additional information to improve the discrimination ability of QUS. The results corresponding to each hypothesis are discussed in the following section.

5.1.1 Hypothesis 1

Hypothesis 1 : The parameters of the homodyned K-distribution from ultrasound echo envelope data are affected by shear wave propagation.

Does shear wave propagation have an effect on the homodyned K-distribution parameters ?

It was the first question of this research study. To answer this question, the time evolution of the homodyned K-distribution parameters during shear wave propagation was investigated via the *in-vitro* experiments. Quantitative analysis was performed by comparing the static and dynamic ranges of the homodyned K-distribution parameters. Two-way ANOVA analysis revealed significant differences between the two types of range, except for the κ parameter in phantom C.

The structure parameter κ of phantom *C* was zero in all the frames except at the time of the push. Therefore, the static and dynamic ranges of the κ parameter were zero and were not distinguishable from each other. This may be attributed to the stiffness of the phantom. Indeed, phantom *C* was stiffer than the other two phantoms, and thus a small displacement field was generated in it. Thus, the κ parameter, which is related to the structure parameter of the scattering medium, may not be affected by small displacements in stiff phantoms, such as phantom *C*, during shear wave propagation. Another issue is that the relative bias and standard deviation of the estimated κ parameter are increased by enlarging the value of the α parameter ($\alpha > 10$) (14). Thus, for large values of α, the estimated κ parameter may be less reliable. Now, the estimated

value of the α parameter for phantom *C* in the static case was around 18. This implies that the estimation of the κ parameter was less reliable in the case of phantom *C*, and hence its estimated value was less sensitive to a small displacement amplitude. In Table 4.III, coefficients of variation of static and dynamic ranges of homodyned K-distribution parameters were presented. These values were larger for static ranges of parameters (0.15 to 0.75) than for dynamic ranges of the same parameters (0.014 to 0.24). Note however, that static ranges of parameters were considered in this study only to demonstrate hypothesis 1. Indeed, in static QUS, one considers the mean or median values of parameters over various frames in a B-mode sequence, rather than their ranges. As one can see from Table 4.VI, the CVs of median values of the considered statistical parameters over 5 frames were at most 0.022. Thus, median values of these parameters are likely to be more reliable than their ranges in static QUS. Overall, the results showed a significant difference between the static and dynamic range of the homodyned K-distribution parameters for the phantoms with $p < 0.001$.

5.1.2 Hypothesis 2

Hypothesis 2 : The range of the parameters of the homodyned K-distribution during shear wave propagation can be used to discriminate different tissue mimicking phantoms.

The second hypothesis was related to the ability of dynamic QUS to discriminate between tissue mimicking phantoms. The static values of the homodyned K-distribution parameters were compared with the dynamic range of these parameters. From two-way ANOVA analysis was performed on the static values and the dynamic range of the homodyned K-distribution parameters obtained from the three *in-vitro* phantoms. This analysis revealed that the dynamic range of the parameters could distinguish between the three phantoms, except for phantoms *B* and *C* in the case of the α parameter.

The dynamic range of the α parameter did not discriminate between phantoms *B* and *C*. This may be due to the fact that the two-way ANOVA test was applied on the three phantoms together. Indeed, it is seen in Table 4.IV that the values of the α parameter for phantoms *B* and *C* are one order of magnitude smaller than that for phantom *A*. Thus, the values of the α parameter

for phantoms B and C are not significantly different, when that of phantom A is considered. To prove this point, a one-way ANOVA test was performed on the dynamic range of α for only phantoms B and C. This test showed that the dynamic range of the α parameter could discriminate between the two phantoms with $p < 0.001$. Note that in a specific application, one may not need to discriminate all the tissues from each other. As an example, if phantom A represents a benign tumor and the two other phantoms are mimicking malignant tumors, then the goal would be to differentiate A from B and C, rather than distinguishing B from C.

The two-way ANOVA tests also showed that the median values of the statistical parameters could distinguish between the three phantoms. But note that static QUS is expected to reveal information about the microstructure of tissues (number of scatterers, their spatial organization and their acoustical properties), whereas dynamic QUS would be related to mechanical properties of tissues. See section 5.1.3 for additional results on this matter.

The results in this section showed that, depending on the application, dynamic QUS can help tissue discrimination.

5.1.3 Hypothesis 3

Hypothesis 3 : The maximal displacement amplitude of the medium and the reciprocal of the Young's modulus are correlated with the range of the parameters of the homodyned K-distribution during shear wave propagation.

Relations between mechanical properties of the scattering medium and statistical parameters of the homodyned K-distribution were investigated as formulated with the third hypothesis. A linear regression test was performed between the static values or the dynamic range of the homodyned K-distribution parameters and the maximum displacement amplitude or the $1/E$ parameter. We postulated that by increasing phantom stiffness, and hence decreasing the maximum displacement amplitude of the medium, statistical parameters would be less affected by shear wave propagation, resulting in a smaller range.

According to Tables 4.VIII and 4.IX, overall, dynamic QUS in comparison with static QUS is more correlated with the mechanical properties for the three phantoms. Again, static QUS is expected to be related to the microstructure of the medium, rather than its mechanical properties.

The R^2 coefficients of determination of the linear regressions between the dynamic range of the homodyned K-distribution parameters and the maximal displacement amplitudes were larger than that of the linear regressions with $1/E$. Finally, one can see that the best linear regression occurred for the case of the dynamic range of the μ parameter and the maximum displacement amplitude with an R^2 coefficient of determination of 0.98 and $p < 0.001$.

In conclusion, dynamic QUS parameters were correlated with the maximum displacement amplitude and the $1/E$ parameter for all the *in-vitro* phantoms, whereas such a correlation was substantially smaller for the static QUS parameters.

5.1.4 Hypothesis 4

Hypothesis 4 : Dynamic QUS can help in distinguishing the mice tumors from their surrounding medium.

The next step was to use the dynamic QUS to distinguish the mice tumors from their surrounding medium. Analysis of the *ex-vivo* results showed that the estimated homodyned K-distribution parameters within the tumor were affected by shear wave propagation. Two-way ANOVA test showed that static and dynamic QUS could distinguish the tumors from their surrounding medium, but based on different types of information.

5.1.5 Hypothesis 5

Hypothesis 5 : The maximal displacement amplitude of the mice tumors is correlated with the range of the parameters of the homodyned K-distribution during shear wave propagation.

Finally, the last hypothesis concerned correlations between dynamic or static QUS parameters and mechanical properties of the mice tumors or their surrounding agar gelatin medium. According to Tables 4.XIII, dynamic QUS in comparison with static QUS was not always more correlated with the maximal displacement amplitude for the tumors. Nevertheless, the maximal

R^2 coefficient of determination occurred for the dynamic range of the μ parameter with a value of 0.56 and p = 0.013. Moreover, Table 4.XIV indicates that dynamic QUS in comparison with static QUS was more correlated with the mechanical properties for the surrounding agar gelatin material. The maximum R^2 coefficient of determination occurred for the dynamic range of the μ parameter with a value of 0.59 and p = 0.009.

Considering the *in-vitro* and *ex-vivo* results, the dynamic range of the μ parameter was the most significantly correlated with the maximal displacement amplitude during shear wave propagation.

5.2 Limitations of the study

In this study, the number of phantoms and mice tumors was small. In order to have a better statistical analysis, the sample size of phantoms and mice tumors should be increased.

According to Table 3.I, a wide range of elasticities of breast lesions were reported in previous studies. Thus, in the *in-vitro* experiments, one might consider a wider range of Young's modulus for the agar gelatin medium.

In this study, the mice tumors were malignant with same type of cancer cells. A further research topic would be to assess the ability of dynamic QUS to discriminate benign from malignant tumors. Moreover, the surrounding medium in the *ex-vivo* experiments were fabricated with agar gelatin and were stiffer than the mice tumors. However, malignant tumors are usually stiffer than surrounding breast tissues (62). Therefore, to have more realistic experiments, it would be instructive to consider a softer surrounding medium in the *ex-vivo* experiments.

The pushing time in the SSI method for the shear wave generation is limited. This is due to the fact that the radiation force is a highly focused beam and by increasing the pushing time, the temperature of the medium is increased. The pushing time cannot be increased more than a specific threshold to prevent damages in mechanical properties of the phantoms due to the temperature rise and a potential damage to the phantom. Thus, the maximal displacement amplitude is limited and the effect of the shear wave on the homodyned K-distribution parameters may not be significant in stiff phantoms that have smaller displacement amplitude during shear wave propagation compared to the soft ones. In fact, according to the results of the *in-vitro* experiments, the range of the κ parameter was 0 in the case of the stiffest phantom, which suggests that this parameter might not be affected by small displacements within stiff medium during shear wave propaga-

tion. On the other hand, it would be interesting to assess if such a behavior of the κ parameter could be used as a marker of stiffness of the medium, in the context of a specific application.

Finally, the manual segmentation for defining the region of interest in the *ex-vivo* experiments could be replaced by automatic or semi-automatic algorithms, such as can be found in (44). This could help control the reproducibility of segmentations of tumors contours.

5.3 Clinical impact

In this study, shear waves were remotely generated by a linear array transducer using the SSI method. Plane wave imaging with a high frame rate allowed rapid acquisition of the images. The computational time for the estimation of the homodyned K-distribution parameters was equal to 6.8 ms per image (14). Therefore, the proposed method to estimate the dynamic behavior of the homodyned K-distribution parameters might be suitable for *in-situ* clinical applications, granted that a segmentation algorithm would be used to delineate the tumors contours. In dynamic elastography, there is no need to segment the tumors. However, a cross-correlation algorithm is needed to compute the displacement map, and without GPU implementation, such an algorithm is more time consuming (few minutes) (41). Thus, the computational time is not so different in dynamic QUS and dynamic elastography.

Note that the goal is not to replace dynamic elastography with dynamic QUS, but to add extra information to current methods that are already amenable to clinical applications. Related to this matter, one would need to assess the improvement on precision, sensitivity and specificity brought by dynamic QUS to the current dynamic elastography and QUS methods. One should also study reproducibility of dynamic QUS based on variations of the tumors segmentations.

5.4 Future studies

In order to prove the concept of dynamic QUS, we presented the experimental results obtained from the *in-vitro* and *ex-vivo* experiments. For future work, the number of phantoms may be increased. We suggest to consider a surrounding medium softer than the tumors for the *ex-vivo* experiments. Moreover, using an automatic segmentation algorithm instead of manual segmentation for *ex-vivo* experiments is recommended.

It is interesting to analytically investigate the scatterers behavior during shear wave propagation. This may be performed through the homodyned K-distribution. The first step may be

to assess the behavior of the α parameter during the shear wave propagation. The α parameter may be interpreted as the effective density of the scatterers (43) that is defined by the following equation :

$$\alpha = \alpha_0 * N, \tag{5.1}$$

where α_0 is a measure of homogeneity of the scattering medium and N is the number of scatterers per resolution cell (43). The parameter N can be assumed constant during plane shear wave propagation, as the number of scatterers is supposedly the same in a specific ROI. Therefore, based on the interpretation suggested in (43), studying the dynamic behavior of the α_0 parameter during shear wave propagation may be one approach to investigate the effective density of scatterers.

Moreover, the linear regression between mechanical properties and the static value or the dynamic range of the κ parameter suggests that the microstructure of the phantoms may vary during shear wave propagation. In particular, an analytical study of the κ parameter needs to be performed to understand how shear wave propagation affects the microstructure of the medium.

The results obtained from the *in-vitro* and *ex-vivo* experiments showed a significant linear regression between the range of the mean intensity under shear wave propagation and the maximal displacement amplitude. This suggests to analytically study the behavior of the mean intensity of the echo envelope during shear wave propagation.

5.5 Summary and conclusion

Supersonic shear imaging (SSI) method was used to produce shear wave inside 3 *in-vitro* and 2 *ex-vivo* phantoms and the RF data was acquired with the plane wave imaging technique. The results obtained from these *in-vitro* and *ex-vivo* experiments showed that the parameters of the homodyned K-distribution as a general model of the ultrasound backscattering echo envelope were affected by shear wave propagation due to the changes in the microstructure of the media. Dynamic QUS was overall as powerful as static QUS to distinguish between the three *in-vitro* phantoms with different structural and mechanical properties and the mice tumors from their surrounding medium with $p < 0.001$. The correlation between the mechanical properties and the dynamic QUS parameters was investigated by a linear regression model. The results showed a significant linear regression between the range of the mean intensity under shear wave propagation and maximum displacement amplitude (*in-vitro* phantoms : R^2 coefficient of determination

= 0.98, $p < 0.001$; *ex-vivo* tumors : $R^2 = 0.56$, $p = 0.013$; *ex-vivo* surrounding medium : $R^2 = 0.59$, $p = 0.009$.). In the case of static QUS, the R^2 coefficient of determination of the linear regression between the mean intensity and mechanical properties of the medium was not significant (*in-vitro* phantoms : $R^2 = 0.07$, $p = 0.328$, *ex-vivo* tumors : $R^2 = 0.55$, $p = 0.022$; *ex-vivo* surrounding medium : $R^2 = 0.45$, $p = 0.047$).

On a long term basis, this work aimed at assessing if statistical QUS parameters under shear wave propagation (dynamic QUS) could increase the discriminant power of ultrasound imaging techniques used for breast tissue characterization and differentiation of benign and malignant tumors. The current study showed the feasibility of tissue classification using dynamic QUS, related to tissue mechanical properties and the changes in their microstructure under shear wave propagation. The preliminary results presented in the appendices showed an example where dynamic QUS was able to distinguish an inclusion from its surrounding medium, while static QUS was not able to do so. Considering the presented results, dynamic QUS may be considered as a new approach to provide additional information to static QUS with potential application in breast lesion classification.

BIBLIOGRAPHIE

[1] M. Alavi, F. Destrempes, E. Montagnon, and G. Cloutier. Dynamic quantitative ultrasound imaging of mimicked breast lesions during shear wave propagation to emphasize differences in tissue statistical backscatter properties. In *Proceedings of Meetings on Acoustics*, volume 19, pages 1–6. Acoustical Society of America, 2013.

[2] M. Alavi, F. Destrempes, C. Schmitt, E. Montagnon, and G. Cloutier. Shear wave propagation modulates quantitative ultrasound K-distribution echo envelope model statistics in homogeneous viscoelastic phantoms. In *IEEE International Ultrasonics Symposium (IUS)*, pages 2348–2351, 2012.

[3] R. Andreesen, C. Scheibenbogen, W. Brugger, S. Krause, H. G. Leser, S. Kopf, H. Engler, C. Schümichen, and G. W. Löhr. A new approach to adoptive immunotherapy of cancer using tumorcytotoxic macrophages grown from peripheral blood monocytes. *Cancer Detection and Prevention*, 15(5) :413–415, 1991.

[4] S. R. Benson, J. Blue, K. Judd, and J. E. Harman. Ultrasound is now better than mammography for the detection of invasive breast cancer. *The American journal of surgery*, 188(4) :381–385, 2004.

[5] W. A. Berg. Benefits of screening mammography. *Journal of the American Medical Association (JAMA)*, 303(2) :168–169, 2010.

[6] W. A. Berg, J. D. Blume, J. B. Cormack, E. B. Mendelson, D. Lehrer, M. Böhm-Vélez, E. D. Pisano, R. A. Jong, W. P. Evans, M. J. Morton, M. C. Mahoney, L. H. Larsen, R. G. Barr, D. M. Farria, H. S. Marques, and K. Boparai. Combined screening with ultrasound and mammography vs mammography alone in women at elevated risk of breast cancer. *Journal of the American Medical Association (JAMA)*, 299(18) :2151–2163, 2008.

[7] W. A. Berg, D. O. Cosgrove, C. J. Doré, F. K. Schäfer, W. E. Svensson, R. J. Hooley, R. Ohlinger, E. B. Mendelson, C. Balu-Maestro, et al. Shear-wave elastography improves the specificity of breast US : the be1 multinational study of 939 masses. *Radiology*, 262(2) :435–449, 2012.

[8] J. T. Bushberg, J. A. Seibert, E. M. Leidholdt, and J. M. Boone. *The Essential Physics of Medical Imaging*. Lippincott Williams & Wilkins, 2011.

[9] C. Calderon, D. Vilkomerson, R. Mezrich, K. F. Etzold, B. Kingsley, and M. Haskin. Differences in the attenuation of ultrasound by normal, benign, and malignant breast tissue. *Journal of Clinical Ultrasound*, 4(4) :249–254, 1976.

[10] C. L. Carter, C. Allen, and D. E. Henson. Relation of tumor size, lymph node status, and survival in 24,740 breast cancer cases. *Cancer*, 63 :181–187, 1989.

[11] J. M. Chang, W. K. Moon, N. Cho, A. Yi, H. R. Koo, W. Han, D. Y. Noh, H. G. Moon, and S. J. Kim. Clinical application of shear wave elastography (SWE) in the diagnosis of benign and malignant breast diseases. *Breast cancer research and treatment*, 129(1) :89–97, 2011.

[12] F. Destrempes and G. Cloutier. A critical review and uniformized representation of statistical distributions modeling the ultrasound echo envelope. *Ultrasound in Medicine and Biology*, 36(7) :1037–1051, 2010.

[13] F. Destrempes and G. Cloutier. Review of envelope statistics models for quantitative ultrasound imaging and tissue characterization. In J. Mamou and M. L. Oelze, editors, *Quantitative Ultrasound in Soft Tissues*, pages 219–274. Springer Dordrecht Heidelberg New York London, 2013.

[14] F. Destrempes, J. Porée, and G. Cloutier. Estimation method of the homodyned K-distribution based on the mean intensity and two log-moments. *SIAM Journal on Imaging Sciences*, 6(3) :1499–1530, 2013.

[15] F. Destrempes, G. Soulez, M. F. Giroux, J. Meunier, and G. Cloutier. Segmentation of plaques in sequences of ultrasonic B-mode images of carotid arteries based on motion estimation and Nakagami distributions. In *IEEE International Ultrasonics Symposium (IUS)*, pages 2480–2483, 2009.

[16] V. A. Dumane, P. M. Shankar, C. W. Piccoli, J. M. Reid, V. Genis, F. Forsberg, and B. B. Goldberg. Classification of ultrasonic B mode images of the breast using frequency diversity and Nakagami statistics. *IEEE Transactions on Ultrasonics, Ferroelectrics and Frequency Control*, 49(5) :664–668, 2002.

[17] V. Dutt and J. F. Greenleaf. Ultrasound echo envelope analysis using a homodyned K distribution signal model. *Ultrasonic Imaging*, 16(4) :265–287, 1994.

[18] J. G. Elmore, K. Armstrong, C. D. Lehman, S. W. Fletcher, and W. Suzanne. Screening for breast cancer. *Journal of the American Medical Association (JAMA)*, 293(10) :1245–1256, 2005.

[19] K. Flobbe, P. J. Nelemans, A. G. Kessels, G. L. Beets, M. F. von Meyenfeldt, and J. M. van Engelshoven. The role of ultrasonography as an adjunct to mammography in the detection of breast cancer : a systematic review. *European Journal of Cancer*, 38(8) :1044–1050, 2002.

[20] D. Garcia, L. L. Tarnec, S. Muth, E. Montagnon, J. Porée, and G. Cloutier. Stolt's f-k migration for plane wave ultrasound imaging. *IEEE Transactions on Ultrasonics, Ferroelectrics and Frequency Control*, 60(9) :1853–67, 2013.

[21] J. L. Gennisson and G. Cloutier. Sol-gel transition in agar-gelatin mixtures studied with transient elastography. *IEEE Transactions on Ultrasonics, Ferroelectrics and Frequency Control*, 53(4) :716–723, 2006.

[22] J. F. Greenleaf, M. Fatemi, and M. Insana. Selected methods for imaging elastic properties of biological tissues. *Annual Review of Biomedical Engineering*, 5(1) :57–78, 2003.

[23] P. Greenwald, P. C. Nasca, C. E. Lawrence, J. Horton, R. P. McGarrah, T. Gabriele, and K. Carlton. Estimated effect of breast self-examination and routine physician examinations on breast-cancer mortality. *New England Journal of Medicine*, 299(6) :271–273, 1978.

[24] J. M. Greif. Mammographic screening for breast cancer : An invited review of the benefits and costs. *The Breast*, 19(4) :268–272, 2010.

[25] I. Griebsch, J. Brown, C. Boggis, A. Dixon, M. Dixon, D. Easton, R. Eeles, D. G. Evans, F. J. Gilbert, J. Hawnaur, P. Kessar, S. R. Lakhani, S. M. Moss, A. Nerurkar, et al. Cost-effectiveness of screening with contrast enhanced magnetic resonance imaging vs X-ray mammography of women at a high familial risk of breast cancer. *British journal of cancer*, 95(7) :801–810, 2006.

[26] D. P. Hruska and M. L. Oelze. Improved parameter estimates based on the homodyned K-distribution. *IEEE Transactions on Ultrasonics, Ferroelectrics and Frequency Control*, 56(11) :2471–2481, 2009.

[27] V. P. Jackson. Management of solid breast nodules : what is the role of sonography ? *Radiology*, 196(1) :14–15, 1995.

[28] E. Jakeman. On the statistics of K-distributed noise. *Journal of Physics A : Mathematical and General*, 13(1) :31–48, 1980.

[29] E. Jakeman and R. J. A. Tough. Generalized K-distribution : a statistical model for weak scattering. *Journal of Optical Society of America*, 4(9) :1764–1772, 1987.

[30] F. Kallel, M. Bertrand, and J. Meunier. Speckle motion artifact under tissue rotation. *IEEE Transactions on Ultrasonics, Ferroelectrics and Frequency Control*, 41(1) :105–122, 1994.

[31] T. M. Kolb, J. Lichy, and J. H. Newhouse. Comparison of the performance of screening mammography, physical examination, and breast US and evaluation of factors that influence them : an analysis of 27,825 patient evaluations. *Radiology*, 225(1) :165–175, 2002.

[32] M. Kriege, C. T. Brekelmans, C. Boetes, P. E. Besnard, H. M. Zonderland, I. M. Obdeijn, et al. Efficacy of MRI and mammography for breast-cancer screening in women with a familial or genetic predisposition. *New England Journal of Medicine*, 351(5) :427–437, 2004.

[33] L. Landini and R. Sarnelli. Evaluation of the attenuation coefficients in normal and pathological breast tissue. *Medical and Biological Engineering and Computing*, 24(3) :243–247, 1986.

[34] Y. Y. Liao, C. H. Li, P. H. Tsui, C. C. Chang, W. H. Kuo, K. J. Chang, and C. K. Yeh. Strain-compounding technique with ultrasound Nakagami imaging for distinguishing between benign and malignant breast tumors. *Medical Physics*, 39(5) :2325–33, 2012.

[35] J. C. Litherland, S. Stallard, D. Hole, and C. Cordiner. The effect of hormone replacement therapy on the sensitivity of screening mammograms. *Clinical Radiology*, 54(5) :285–288, 1999.

[36] S. J. Lord, W. Lei, P. Craft, J. N. Cawson, I. Morris, S. Walleser, A. Griffiths, S. Parker, and N. Houssami. A systematic review of the effectiveness of magnetic resonance imaging (MRI) as an addition to mammography and ultrasound in screening young women at high risk of breast cancer. *European Journal of Cancer*, 43(13) :1905–1917, 2007.

[37] H. Madjar and E. Mendelson. *Practice of Breast Ultrasound : Techniques, Findings, Differential Diagnosis*. Thieme, 2008.

[38] Y. K. Mariappan, K. J. Glaser, and R. L. Ehman. Magnetic resonance elastography : a review. *Clinical Anatomy*, 23(5) :497–511, 2010.

[39] M. Mitka. New ultrasound “elasticity" technique may reduce need for breast biopsies. *JAMA : the Journal of the American Medical Association*, 297(5) :455–455, 2007.

[40] R. C. Molthen, P. M. Shankar, J. M. Reid, F. Forsberg, E. J. Halpern, C. W. Piccoli, and B. B. Goldberg. Comparisons of the Rayleigh and K-distribution models using in-vivo breast and liver tissue. *Ultrasound in Medicine and Biology*, 24(1) :93–100, 1998.

[41] E. Montagnon, S. Hissoiny, P. Despres, and G. Cloutier. Real-time processing in dynamic ultrasound elastography : A GPU-based implementation using CUDA. In *11th International Conference on Information Science, Signal Processing and their Applications (ISSPA)*, pages 472–477, 2012.

[42] M. Nakagami. The m-distribution - A general formula of intensity distribution of rapid fading. *In : Hoffman WC (ed) Stat Methods Radio Wave Propag.*, pages 3–36, 1960.

[43] V. M. Narayanan, P. M. Shankar, and J. M. Reid. Non-Rayleigh statistics of ultrasonic backscattered signals. *IEEE Transactions on Ultrasonics, Ferroelectrics and Frequency Control*, 41(6) :845–852, 1994.

[44] J. A. Noble and D. Boukerroui. Ultrasound image segmentation : a survey. *Medical Imaging, IEEE Transactions on*, 25(8) :987–1010, 2006.

[45] M. L. Oelze, W. D. O’Brien, and J. F. Zachary. 11b-4 quantitative ultrasound assessment of breast cancer using a multiparameter approach. In *IEEE Ultrasonics Symposium*, pages 981–984, 2007.

[46] M. L. Oelze, J. F. Zachary, and W. D. O'Brien. Parametric imaging of rat mammary tumors in vivo for the purposes of tissue characterization. *Journal of Ultrasound in Medicine*, 21(11) :1201–1210, 2002.

[47] K. J. Parker, M. M. Doyley, and D. J. Rubens. Imaging the elastic properties of tissue : the 20 year perspective. *Physics in Medicine and Biology*, 56(1) :R1–R29, 2011.

[48] N. H. Peters, R. I. H. Borel, N. P. Zuithoff, W. P. Mali, K. G. Moons, and P. H. Peeters. Meta-analysis of MR imaging in the diagnosis of breast lesions. *Radiology*, 246(1) :116–124, 2008.

[49] G. Rahbar, A. C. Sie, G. C. Hansen, J. S. Prince, M. L. Melany, H. E. Reynolds, V. P. Jackson, J. W. Sayre, and L. W. Bassett. Benign versus malignant solid breast masses : Us differentiation. *Radiology*, 213(3) :889–894, 1999.

[50] L. Rayleigh. On the resultant of a large number of vibrations of the same pitch and of arbitrary phase. *The London, Edinburgh, and Dublin Philosophical Magazine and Journal of Science*, 10(60) :73–78, 1880.

[51] A. Samani, J. Zubovits, and D. Plewes. Elastic moduli of normal and pathological human breast tissues : an inversion-technique-based investigation of 169 samples. *Physics in Medicine and Biology*, 52(6) :1565–76, 2007.

[52] A. P. Sarvazyan, O. V. Rudenko, S. D. Swanson, J. B. Fowlkes, and S. Y. Emelianov. Shear wave elasticity imaging : a new ultrasonic technology of medical diagnostics. *Ultrasound in Medicine and Biology*, 24(9) :1419–1435, 1998.

[53] D. Saslow, C. Boetes, W. Burke, S. Harms, M. O. Leach, C. D. Lehman, E. Morris, E. Pisano, M. Schnall, S. Sener, et al. American cancer society guidelines for breast screening with MRI as an adjunct to mammography. *Cancer Journal for Clinicians (CA)*, 57(2) :75–89, 2007.

[54] D. Schopper and C. D. Wolf. How effective are breast cancer screening programmes by mammography ? review of the current evidence. *European journal of cancer*, 45(11) :1916–1923, 2009.

[55] P. M. Shankar. A general statistical model for ultrasonic backscattering from tissues. *IEEE Transactions on Ultrasonics, Ferroelectrics and Frequency Control*, 47(3) :727–736, 2000.

[56] P. M. Shankar, V. A. Dumane, T. George, C. W. Piccoli, J. M. Reid, F. Forsberg, and B. B. Goldberg. Classification of breast masses in ultrasonic B-scans using nakagami and K-distributions. *Physics in Medicine and Biology*, 48(14) :2229–40, 2003.

[57] P. M. Shankar, J. M. Reid, H. Ortega, C. W. Piccoli, and B. B. Goldberg. Use of non-Rayleigh statistics for the identification of tumors in ultrasonic B-scans of the breast. *IEEE Transactions on Medical Imaging*, 12(4) :687–692, 1993.

[58] R. Sinkus, K. Siegmann, T. Xydeas, M. Tanter, C. Claussen, and M. Fink. MR elastography of breast lesions : Understanding the solid/liquid duality can improve the specificity of contrast-enhanced MR mammography. *Magnetic Resonance in Medicine*, 58(6) :1135–1144, 2007.

[59] A. T. Stavros. *Breast Ultrasound*. Lippincott Williams & Wilkins, 2004.

[60] A. T. Stavros, D. Thickman, C. L. Rapp, M. A. Dennis, S. H. Parker, and G. A. Sisney. Solid breast nodules : use of sonography to distinguish between benign and malignant lesions. *Radiology*, 196(1) :123–134, 1995.

[61] L. Tabar, M. F. Yen, B. Vitak, H. H. T. Chen, R. A. Smith, and S. W. Duffy. Mammography service screening and mortality in breast cancer patients : 20-year follow-up before and after introduction of screening. *The Lancet*, 361(9367) :1405–1410, 2003.

[62] M. Tanter, J. Bercoff, A. Athanasiou, T. Deffieux, J. L. Gennisson, G. Montaldo, M. Muller, A. Tardivon, and M. Fink. Quantitative assessment of breast lesion viscoelasticity : Initial clinical results using supersonic shear imaging. *Ultrasound Med. Biol*, 34(9) :1373–1386, 2008.

[63] I. Trop, F. Destrempes, M. El Khoury, A. Robidoux, L. Gaboury, L. Allard, B. Chayer, and G. Cloutier. The added value of statistical parameters based on sonographic backscattering properties of tissues in the management of breast lesions. *98th Scientific Assembly and Annual Meeting of the Radiological Society of North America, Chicago*, November 25-28 2012.

[64] P. H. Tsui and C. C. Chang. Imaging local scatterer concentrations by the Nakagami statistical model. *Ultrasound in medicine and Biology*, 33(4) :608–619, 2007.

[65] P. H. Tsui, C. K. Yeh, C. C. Chang, and Y. Y. Liao. Classification of breast masses by ultrasonic Nakagami imaging : a feasibility study. *Physics in Medicine and Biology*, 53(21) :6027–44, 2008.

[66] T. Umemoto, E. Ueno, T. Matsumura, M. Yamakawa, H. Bando, T. Mitake, and T. Shiina. Ex vivo and in vivo assessment of the non-linearity of elasticity properties of breast tissues for quantitative strain elastography. *Ultrasound in medicine & biology*, 2014.

[67] R. F. Wagner, S. W. Smith, J. M. Sandrik, and H. Lopez. Statistics of speckle in ultrasound B-scans. *IEEE Transactions on Sonics and Ultrasonics*, 30(3) :156–163, 1983.

[68] E. Warner, H. Messersmith, P. Causer, A. Eisen, R. Shumak, and D. Plewes. Systematic review : using magnetic resonance imaging to screen women at high risk for breast cancer. *Annals of internal medicine*, 148(9) :671–679, 2008.

[69] E. White, P. Velentgas, M. T. Mandelson, C. D. Lehman, J. G. Elmore, P. Porter, Y. Yasui, and S. H. Taplin. Variation in mammographic breast density by time in menstrual cycle among women aged 40–49 years. *Journal of the National Cancer Institute*, 90(12) :906–910, 1998.

[70] B. P. Will, J. M. Berthelot, C. Le Petit, E. M. Tomiak, S. Verma, and W. K. Evans. Estimates of the lifetime costs of breast cancer treatment in canada. *European journal of cancer*, 36(6) :724–735, 2000.

Annexe I

Shear wave propagation modulates quantitative ultrasound K-distribution echo envelope model statistics in homogeneous viscoelastic phantoms (2)

I.1 Abstract

In the context of tissue characterization, one may wonder what does the consideration of a quantitative ultrasound (QUS) feature of a medium under the propagation of a shear wave (SW) add to its discriminant power. This study presents the time-varying behavior of the K-distribution beta parameter - the reciprocal of the effective density of scatterers - under SW propagation and its relation with the viscoelasticity of the medium. Transient plane SW at 300 Hz central frequency was transmitted to three agar-gelatin phantoms at different concentrations. The amplitude of the B-mode backscatter echoes acquired with an 8 MHz probe was modeled with the K-distribution. The normalized range of beta (i.e., its range normalized by its mean value as the SW propagates) was determined by considering the B-mode images during SW propagation. Also, the storage (G') and loss (G'') moduli of each phantom were measured on samples with the RheoSpectris hyper-frequency instrument (Rheolution, Montreal, Canada). The time-evolution of the beta parameter and displacements (using cross-correlation) within tissue-mimicking phantoms under SW vibration suggest that the beta parameter can be used to track SW propagation. *In-vitro* results showed that the normalized range of beta is related to the viscoelasticity of phantoms. By increasing G' and G'', the normalized range of beta decreased. Thus, the consideration of the behavior of beta under SW propagation modifies the effective density of scatterers with respect to static conditions (i.e., without SW). This is new observation and a new step towards understanding statistical QUS behavior.

I.2 Introduction

Breast tissue characterization based on quantitative ultrasound (QUS) has been introduced a few decades ago [1,2]. Optical photomicrographs of breast tissues of mice showed significant differences in microstructure for pathological tissues [3]. Based on that observation, the consideration of differences in diameter or acoustic concentration of cells and nuclei (playing the role of

scatterers) could be used to classify pathological breast tissues [3,4]. Moreover, various models such as the Nakagami or the K-distribution have been proposed to describe the distribution of the ultrasound echo envelope from tissues [5,6]. The homodyned K-distribution is the most general distribution model for ultrasound echo envelopes for which its parameters have a physical interpretation that is compatible with the limit case of a vanishing diffuse signal power, as opposed to other models. Also, it is known that in the case of no coherent component, the homodyned K-distribution amounts to the K-distribution [7]. Recently, Liao *et al.* showed that by combining a strain-compounding technique and the Nakagami model, the specificity of breast tissue classification could be improved [8].

From a mechanical point of view, during 20 years of research in elastography, various methods have been used to estimate tissue viscoelasticity in order to categorize pathological from normal tissues [9]. Elastography methods are characterized as static and dynamic methods. In static elastography, the deformation is detected by applying a force on the tissue. This method has its own limitations due to its operator dependency and the effect of pre-compression force. Therefore, dynamic elastography was proposed as a quantitative method to improve the accuracy of existing approaches. Dynamic elastography based on shear wave propagation was introduced by Sarvazyan et al. [10]. With this method, the shear wave propagates through the medium and the tissue displacement is detected with ultrasound imaging. With proper assumption, the shear wave speed can be related to the elasticity modulus of the medium.

Recently, some studies suggested estimating statistical parameters to determine hardening of porcine lens and rat liver fibrosis [11,12]. By considering these studies, this paper proposes a novel approach in QUS to understand the behavior of ultrasound scatterers under shear wave propagation. The goal is to show the feasibility of combining QUS imaging and dynamic elastography to give new information on tissue properties, with the aim of diagnosing pathological states.

I.3 Theoretical model

I.3.1 Parameter estimation

In the context of ultrasonic tissue characterization, various models have been proposed for the statistical analysis of the ultrasound echo envelope. The homodyned K-distribution is presently the most general model with a consistent physical meaning for modeling the first-order statistics

of the amplitude of the echo envelope. In the absence of a coherent component, the homodyned K-distribution is referred as the K-distribution [7]. The probability density function (pdf) of the K-distribution is expressed as :

$$P_{\mathrm{K}}(A \mid \sigma^2, \alpha) = \frac{4A^{\alpha}}{(2\sigma^2)^{(\alpha+1)/2}\Gamma(\alpha)} K_{\alpha-1}\left(\sqrt{\frac{2}{\sigma^2}}A\right), \tag{I.1}$$

where its two parameters $2\sigma^2$ and α are positive real numbers and correspond to the effective cross section and effective density of the scatterers, respectively, A is the amplitude, K_p denotes the modified Bessel function of the second kind of order p and Γ is the Euler Gamma function.

Another issue which should be considered in the model fitting is the choice of estimators for a specific distribution. For the K-distribution model, it is known that the X-statistics is a better estimator for K-distributed data among other known estimators [13]. That statistics is defined as :

$$X = \frac{\langle I \log I \rangle}{\langle I \rangle} - \langle \log I \rangle. \tag{I.2}$$

Here, I is the intensity of the backscatter echo envelope (i.e., the square of its amplitude A) and the symbol $\langle \cdot \rangle$ denotes the average over a sample of a random variable. Then, one sets

$$\alpha = \frac{1}{X-1}. \tag{I.3}$$

In the case where $X \leq 1$, α becomes meaningless. To avoid this problem, the parameter β (the reciprocal of the parameter α) was proposed [14] and β is assumed to be zero whenever $X \leq 1$ [15].

I.3.2 Shear wave propagation

Consider a plane shear wave which is polarized in the y direction and propagates in the x direction in a homogeneous, linear viscoelastic and incompressible medium. The complex stationary displacement (U) is :

$$U_y(x) = U_0 e^{i(k'+ik'')x} e^{i\phi}, \tag{I.4}$$

where U_0 is the absolute value of the wave amplitude, ϕ is an arbitrary phase, and k' and k'' represent the real and the imaginary part of the complex wave number. Also, the complex shear

modulus (G^*) is related to the complex wave number as :

$$G^* = G' + iG'' = \rho \frac{2\pi f_{sw}}{(k' + ik'')^2}, \tag{I.5}$$

where ρ and f_{sw} are the density of the medium and the frequency of shear wave, respectively. G' is the storage modulus which corresponds to the elastic part and G'' is the loss modulus which is related to the viscous behavior of the medium [16].

I.4 Method

Three cubic agar-gelatin viscoelastic phantoms were made. The concentration of agar and gelatin and the shear moduli of each phantom is given in Table 1. A rigid plate was placed in contact with the vibrator (model 4810, Bruel & Kjaer) which applied a plane transient shear wave at 300 Hz central frequency into the phantom. A clinical ultrasound array transducer (L14-5/38, Ultrasonix) of a Sonix RP scanner (Ultrasonix Medical Corporation, Burnaby, BC, Canada) was used for ultrasound imaging and recording of radio-frequency (RF) data. The central frequency of the probe and the sampling frequency were 8 MHz and 40 MHz, respectively. The acquisition depth was 80 mm and the focal depth was 40 mm for each phantom. The storage (G') and loss (G'') moduli of phantom samples were measured with the RheoSpectris hyper-frequency instrument (Rheolution, Montreal, Canada) by transmitting transient shear waves into the samples and measuring displacements using a high sensitive laser sensor [17].

I.5 Results

Assuming no periodic scatterers in the agar-gelatin phantoms, the K-distribution was used to model the ultrasound echo envelope of backscatter echoes. Figure I.1 shows the histogram of reconstructed B-mode images (i.e., from acquired RF data) for one of the agar-gelatin phantoms. The histogram fits very well with the pdf of the estimated K-distribution. The parameters of the pdf were estimated with the X-statistics. Considering vertical windows with the same size ($1/3$ of the whole B-mode image for each window), one can track the propagation of the shear wave within the phantom (Figure I.2). Moreover, Figure I.3 shows the time evolution of the parameter β under shear wave propagation, as well as the displacement of the central point of agar-gelatin phantom which is calculated by a cross-correlation algorithm.

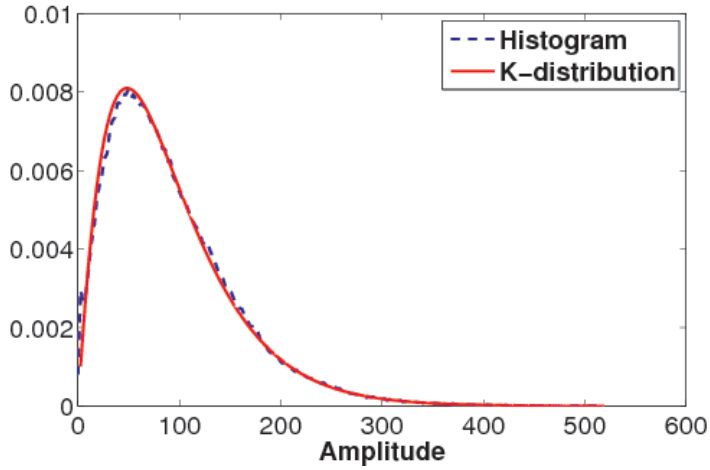

FIGURE I.1 – Histogram of the echo envelope and the estimated K-distribution pdf for the agar 1% - gelatin 3% phantom.

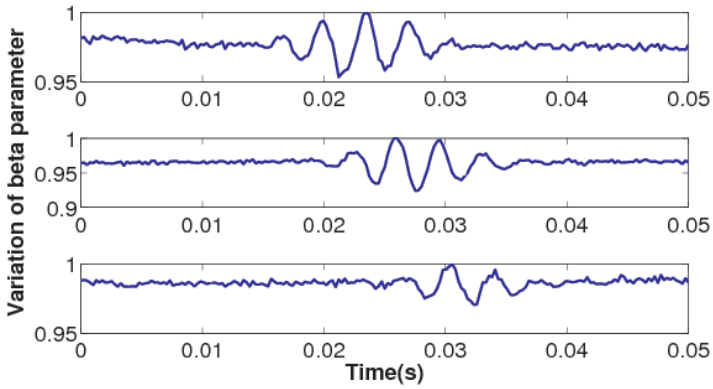

FIGURE I.2 – Time evolution of the beta parameter under shear wave propagation in three different vertical windows (i.e., depth) of equal size.

Table I.I shows the mean value, as well as the normalized range of the parameter β during shear wave propagation. The corresponding viscoelasticity moduli of each phantom are also presented. Displacements of the central point of agar-gelatin phantoms are 4.97, 3.51 and 2.24 μm for concentrations of $5\% - 3\%$, $1\% - 6\%$ and $1\% - 3\%$ agar-gelatin, respectively.

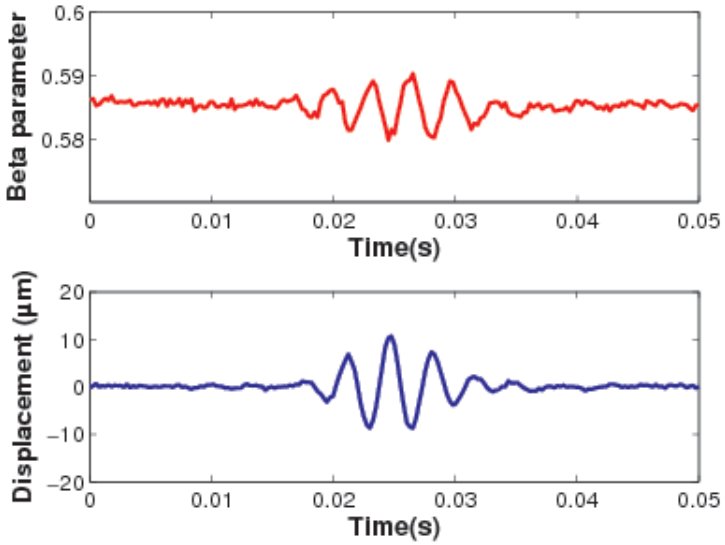

FIGURE I.3 – Variation of the beta parameter with corresponding displacement of the central point of the agar 1% - gelatin 3% phantom.

I.6 Discussion

On a long term basis, this work aims assessing QUS features under shear wave propagation for breast tissue characterization. Mechanical properties of breast tissue mimicking phantoms were chosen to mimic a wide range of pathological breast tissues [18].

Compared with standard QUS methods applied on static images, the results showed the possibility of extracting new information from the time evolution of statistical parameters during shear wave propagation. The variation of the parameter β had a similar pattern as the displacement map. Therefore, it motivated us to verify a possible relation between mechanical properties of phantoms and the time evolution of statistical parameters, reflecting the structure of medium. According to Table I.I, a trend could be seen between the normalized range of the parameter β and the viscoelasticity of agar-gelatin phantoms. As the parameter β reveals information about the homogeneity of the medium, the evolution of that parameter under shear wave propagation could be interpreted by considering the change in the scatterers' spatial organization. Moreover, the mean value of the parameter β was not related to the viscoelasticity of the phantoms. Therefore, the time evolution of the parameter β could give more information than its average value.

TABLE I.I – Behavior of the statistical parameter $\beta = 1/\alpha$ of the K-distribution and mechanical properties (storage and loss moduli G' and G'') of agar-gelatin phantoms.

Proportion of agar-gelatin	G' and G'' (KPa)	Mean value of $\beta = 1/\alpha$	Normalized range of $\beta = 1/\alpha$
5%-3%	22, 2.2	0.6131	0.0090
1%-6%	10, 0.744	0.7013	0.0126
1%-3%	1.6, 0.506	0.5852	0.0179

We also considered the average value of $2\sigma^2\alpha$, the intensity (the square of the amplitude) computed over the whole region of interest , which can be interpreted as the total signal power, and its time evolution during shear wave propagation. Its mean value over the sequence and its normalized range are reported in Table I.II.

According to that table, the dynamic behavior (the normalized range) of the total signal power could not be related to the viscoelasticity of the phantoms.

We conclude that from these observations, the parameter β is a relevant parameter to consider. This approach still needs a theoretical model to interpret the time evolution of the statistical parameters and the effect of physical parameters. Considering heterogeneous media, periodic scatterers corresponding to collagen fibers in breast tissues and the parameters of the homodyned K-distribution as the general distribution model for ultrasound envelope backscatter are future steps in this work.

I.7 Conclusion

Reported *in-vitro* results showed that the normalized range of the parameter β is related to the viscoelasticity of phantoms. An increase in G' and G'' reduced the normalized range of β, which is related to changes in the effective density of scatterers. Thus, the consideration of the behavior of β range under SW propagation gives new information not addressed, to our knowledge, in the literature on QUS imaging. This original study provides new directions to improve soft tissue characterization with ultrasound.

TABLE I.II – Behavior of the statistical parameter $2\sigma^2\alpha$ of the K-distribution and mechanical properties of agar-gelatin phantoms.

Proportion of agar-gelatin	G' and G'' (KPa)	Mean value of $2\sigma^2\alpha$	Normalized range of $2\sigma^2\alpha$
5%-3%	22, 2.2	1.96×10^4	0.0035
1%-6%	10, 0.744	0.61×10^4	0.0063
1%-3%	1.6, 0.506	1.29×10^4	0.0038

Acknowledgments

This work was jointly supported by grants from the Natural Sciences and Engineering Research Council of Canada (# 365656-09) and the Canadian Institutes of Health Research (CPG-95288).

I.8 References

1. C. Calderon, D. Vilkomerson, R. Mezrich, K. F. Etzold, B. Kingsley, and M. Haskin, "Differences in the attenuation of ultrasound by normal, benign and malignant breast tissue," J. Clinical Ultrasound, vol. 4, pp. 249-254 (1976).

2. L. Landini and R. Sarnelli, "Evaluation of the attenuation coefficients in normal and pathological breast tissue," Medical and Biological Engineering and Computing, vol.24, no. 3, pp. 243-247 (1986).

3. M. L. Oelze, W. D. O'Brien, and J. F. Zachary, "Quantitative ultrasound assessment of breast cancer using a multiparameter approach," Proceedings of the 2007 IEEE Ultrasonics Symposium, 981-984 (2007).

4. M. L. Oelze, J. F. Zachary, and W. D. O'Brien, Jr., "Characterization of tissue microstructure using ultrasonic backscatter : Theory and technique for optimization using a gaussian form factor," J. Acoust. Soc. Am., vol. 112, no. 3, pp. 1202-1211 (2002).

5. P. M. Shankar, J. M. Reid, H. Ortega, C. W. Piccoli, and B. B. Goldberg, "Use of non-Rayleigh statistics for the identification of tumors in ultrasonic B-scans of the breast", IEEE

Trans. on Medical Imaging, 12, 687-692 (1993).

6. P. M. Shankar, V. A. Dumane, J. M. Reid, V. Genis, F. Forsberg, C. W. Piccoli, and B. B. Goldberg, "Classification of ultrasonic B-mode images of breast masses using Nakagami distribution," IEEE Trans. Ultrason. Ferroelectr. Freq. Control., vol. 48, no. 2, pp. 569-580 (2001).

7. F. Destrempes and G. Cloutier, "A critical review and uniformized representation of statistical distributions modeling the ultrasound echo envelope," Ultrasound in Medicine & Biology, 36, 1037-1051 (2010).

8. Y. Y. Liao, C. H. Li, P. H. Tsui, C. C. Chang, W. H. Kuo, K. J. Chang and C. K. Yeh, "Strain-compounding technique with ultrasound Nakagami imaging for distinguishing between benign and malignant breast tumors," Medical Physics, 39, 2325-2333 (2012).

9. K. J. Parker, M.M. Doyley, D.J. Rubens, "Imaging the elastic properties of tissue : the 20 year perspective," Physics in Medicine and Biology, 56, R1-R29 (2011).

10. A. P. Sarvazyan, O. V. Rudenko, S. D. Swanson, J. B. Fowlkes, and S. Y. Emelianov, "Shear wave elasticity imaging : A new ultrasonic technology of medical diagnostics," Ultrasound Med. Biol., vol. 24, no. 9, pp. 1419-1435 (1998).

11. P. H. Tsui, C. Huang, Q. Zhou and K.K. Shung, "Cataract measurement by estimating the ultrasonic statistical parameter using an ultrasound needle transducer : an in vitro study," Physiological Measurement, 32, 513-522 (2011).

12. M. C. Ho, J. J Lin, Y. C. Shu, C. N. Chen, K. J. Chang, C. C. Chang and P. H. Tsui., "Using ultrasound Nakagami imaging to assess liver fibrosis in rats," Ultrasonics, 52, 215-222 (2012).

13. D. Blacknell and R. J. A. Tough, "Parameter estimation for the K-distribution based on [z log (z)]", IEE Proc. Radar, Sonar Navig., 148, 309-312 (2001).

14. V. Dutt and J. F. Greenleaf, "Ultrasound echo envelope analysis using a homodyned K distribution signal model," Ultrasonic Imaging, 16, 265-287 (1994).

15. F. Destrempes and G. Cloutier, "Review of envelope statistics models for quantitative ultrasound imaging and tissue characterization," in Quantitative Ultrasound in Soft Tissues, J. Mamou and M. L. Oelze, Springer (New York) (2012).

16. C. Schmitt, A. Hadj Henni, and G. Cloutier, "Ultrasound dynamic micro-elastography applied to the viscoelastic characterization of soft tissues and arterial walls," Ultrasound Med. Biol., vol. 36, no. 9, pp. 1492-1503 (2010).

17. A. Hadj Henni, C. Schmitt, M. E. Tremblay, M. Hamdine, M. C. Heuzey, P. Carreau, and

G. Cloutier, "Hyper-frequency viscoelastic spectroscopy of biomaterials," Journal of the Mechanical Behavior of Biomedical Materials, vol. 4, no. 7, pp. 1115-1122 (2011).

18. M. Tanter, J. Bercoff, A. Athanasiou, T. D. J. L. Gennisson, G.Montaldo, M. Muller, A. Tardivon, and M. Fink, "Quantitative assessment of breast lesion viscoelasticity : Initial clinical results using supersonic shear imaging," Ultrasound Med. Biol., vol. 34, no. 9, pp. 1373-1386 (2008).

Annexe II

Dynamic quantitative ultrasound imaging of mimicked breast lesions during shear wave propagation to emphasize differences in tissue statistical backscatter properties (1)

II.1 abstract

The main motivation was to increase the accuracy of the breast tissue characterization by combining quantitative ultrasound (QUS) with ultrasound (US) dynamic elastography. An agar-gelatin breast mimicking phantom with two inclusions containing the same density of agar (US scatterers) but different proportions of gelatin corresponding to different mechanical properties was made. Transient plane shear waves (SW) at 200 Hz were transmitted through the phantom while the displacement of scatterers was imaged at 5 MHz with an ultrafast imaging technique. From segmented inclusions, the reciprocal (βparameter) of the effective density of scatterers of a general distribution model of the echo envelope and its normalized range (normalized by the mean of β during SW propagation) were estimated for each inclusion. The results showed that the relative difference of β magnitudes between the surrounding medium and both inclusions *A* and *B* were 65.4% (*A*) and 6.4% (*B*), respectively, whereas differences (in %) of the β normalized range (under SW propagation) were 35.3% (*A*) and 35.1% (*B*), respectively. The static value β could barely distinguish inclusion *B* from the surrounding ; however, the dynamic range of β succeeded in that task for both inclusions. Thus, dynamic QUS might add information to QUS performed traditionally in a static framework.

II.2 Introduction

According to the National Cancer Institute of Canada, breast cancer is the most common cancer among Canadian women. In 2012, an estimated 22,700 women were diagnosed and around 5,100 died of breast cancer in Canada. Statistically, an average of 14 women die of breast cancer every day [1]. Early diagnosis is the key issue in optimal treatment [2].The non-invasive diagnostic methods for breast cancer that are used by clinicians are categorized in three groups : X-ray mammography, magnetic resonance imaging (MRI) and ultrasound echography. X-ray mam-

mography is recommended as an annual breast evaluation to women 40 years of age or older. However, the performance of the mammography is poor on women with dense breast and this imaging modality is unable to determine benign breast lesions from malignant ones. In order to provide a complement to mammography, it is suggested to add ultrasound echography [3]. In fact, the main goal of the breast ultrasound examination is to reduce the large number of irrelevant biopsies required to confirm malignancy, and to detect lesions that could be missed by mammography [4]. In the field of ultrasound screening, the variable interpretation of radiological images requires a well-trained and skilled radiologist. Thus, developing quantitative criteria is relevant in that context. Microscopic images have shown the different structures of breast cells in pathological tissues [5]. The rationale behind statistical quantitative ultrasound (QUS) is that the spatial organization of the cell nuclei and their scattering properties leave a signature on the statistical parameters [6]. A variety of statistical distribution models of ultrasound echo envelope (i.e., grayscale of the uncompressed B-mode image) have been used in the field of tissue characterization [7]. Furthermore, multiple approaches in the field of QUS have been applied on breast pathological tissues and could show a significant difference between lesion types [8, 9]. However, the specificity of these statistical methods applied to breast lesion classification as benign or malignant ones is still low. From a mechanical point of view, the early warning sign of breast cancer for the clinician is the stiffness of the tumor, which can be detected by palpation. Various methods in ultrasound elastography imaging have been proposed to estimate the viscoelasticity of tissues to distinguish pathological from normal tissues. In ultrasound dynamic elastography, a shear wave propagates through the medium and the displacement (or velocity) is imaged using ultrasound [10]. Considering the equation of wave propagation, one can estimate the elastic and viscous moduli with this approach [11]. However, this method cannot directly detect any information about the spatial organization of cells, which is not the objective of elastography. Recently, a study showed that combining the strain-compounding technique and statistical parameter estimation could reduce the false negative rate in diagnosing breast cancers [12]. Moreover, some researchers suggested estimating statistical parameters (Nakagami shape parameter) to determine hardening of porcine lens (Young modulus) and also to grade rat liver fibrosis [13, 14]. These studies motivated us to propose a novel approach by considering the behavior of statistical parameters under shear wave propagation, which may provide additional information to standard QUS. In this paper, we show the feasibility of combining the statistical QUS with shear wave propagation in order to have a better classification between two inclusions and their

surrounding medium in a mimicking viscoelastic breast phantom. An example of *in-vitro* experiment revealed that considering a general model of ultrasound echo envelope and the dynamic range of a statistical parameter (the β parameter of the K-distribution) could make a distinction between an inclusion and its surrounding medium, whereas the static value of that parameter was not capable to differentiate between the inclusion and the surrounding medium. Thus, we suggest that this new approach can improve the specificity of ultrasound imaging by providing additional information, which may yield a more efficient diagnosis of breast cancer.

II.3 Method

II.3.1 Envelope Statistics Model

In the context of QUS, it was shown that the homodyned K-distribution is a general distribution model of ultrasound echo envelope with a physical interpretation of its parameters [15]. In the absence of a coherent signal component, the general model is referred to as the K-distribution. Therefore, we assume here that in the case of random scatterers, the K-distribution is a general distribution model of the echo envelope of radio frequency (RF) data. The probability density function (PDF) of the K-distribution is described as [15] :

$$P_{\mathrm{K}}(A \mid \sigma^2, \alpha) = \frac{4A^{\alpha}}{(2\sigma^2)^{(\alpha+1)/2}\Gamma(\alpha)} K_{\alpha-1}\left(\sqrt{\frac{2}{\sigma^2}}A\right), \tag{II.1}$$

Here, K_p is the modified Bessel function of the second kind, of order p, A is the amplitude of the ultrasound echoes, and Γ is the Euler Gamma function. The shape and the scale parameters of the K-distribution can be defined as :

$\alpha = N\alpha_0$ = effective density (shape parameter)

$2\ \sigma^2$ = effective cross section (scale parameter)

where N is the number of scatterers within a resolution cell and α_0 is a parameter describing the homogeneity of the cross-section [14]. For the K-distributed model, it was shown that the X-statistic is a better estimator among other known estimators and is defined as [16] :

$$X = \frac{\langle I \log I \rangle}{\langle I \rangle} - \langle \log I \rangle. \tag{II.2}$$

Here, <I> represents the mean value of the intensity I of the ultrasound echoes. Then, one sets :

$$\alpha = \frac{1}{X - 1}. \tag{II.3}$$

The parameter $\beta = 1/\alpha$ was proposed in [17] in the context of the homodyned K-distribution and can be used to avoid having a meaningless value of α whenever $X \leq 1$. Namely, the parameter β is assumed to be zero whenever $X \leq 1$.

II.3.2 Experiment

Figure II.1 shows the schematic diagram of the experimental set-up. A cubic box was filled with agar-gelatin material (2% agar and 3% gelatin). Breast lesions were mimicked by two hard cylindrical inclusions with 1 cm diameter, which were made by different agar and gelatin percentages (inclusion A : 4% agar with 6% gelatin and inclusion B : 4% agar with 4% gelatin). Transient plane shear waves were transmitted by a function generator (model 33250 A, Agilent, Palo Alto, CA, USA) and supplied by a vibrator (model 4810, Bruel&Kjaer, Naerum, Denmark). A rigid plate was placed in contact with the vibrator, which applied shear waves at 200 Hz frequency into the phantom. A Verasonics V-1 (Verasonics, Redmond, WA, USA) scanner was used for plane wave ultrasound imaging and to record the radio frequency (RF) data. The ultrasound probe was an array transducer ATL (L7-4) with 128 elements, 38 mm width at 5 MHz central frequency.

II.4 Results

Ultrafast imaging was conducted by using the migration process to build B-mode images from the recorded RF data at a very high frame rate [18]. By applying the normalized cross correlation algorithm, the displacement map could be obtained during the shear wave propagation. The evolution of the displacement map along the wave propagation path could show the boundary of an inclusion, because the inclusion presented a shear wave speed that was different from that in the surrounding medium. Based on this property, we superimposed the B-mode image and the displacement map to visualize the inclusions, which allowed segmenting its elliptical shape. Based on these segmentations, the histograms of the B-mode amplitude were calculated for the surrounding medium and both inclusions. The region of interest for the surrounding medium was selected on the left of the inclusions (Figure II.1), where the shear wave was not disturbed by its

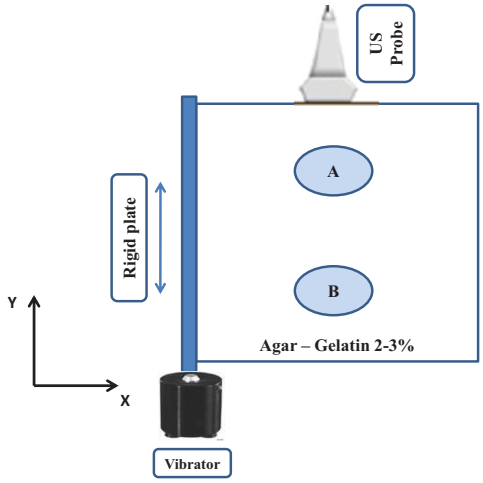

FIGURE II.1 – Schematic diagram of the phantom with two agar-gelatin hard inclusions : A rigid plate vibrates along Y axis and plane shear waves were propagated in the X direction.

interaction with the interface of the mimicking lesions. The PDFs of the K-distribution were estimated using the X-statistics estimator. The model fitting for the three media is shown in Figure II.2.

TABLE II.I – The β parameter of the K-distribution over the three considered media in static mode.

Surrounding medium 2% agar- 3% gelatin	Inclusion A 4% agar- 6% gelatin	Inclusion B 4% agar- 4% gelatin
0.1100	0.0381	0.1175

RF data were recorded in static and dynamic SW modes. The values of the β parameter of the K-distribution in the static case are seen in Table II.I. During shear wave propagation, the β parameter varied over time and depicted a temporal motion similar to the tissue displacement map. The range of β in SW mode was normalized by its mean value during the wave propagation (Table II.II). In this case, both inclusions *A* and *B* presented contrast with respect to the surrounding medium.

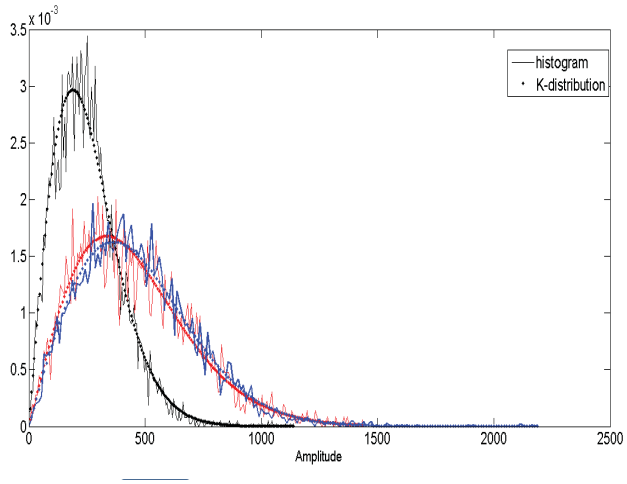

FIGURE II.2 – Histograms of the ultrasound echo envelopes (line) and the estimated PDFs of the K-distribution (points) for the three considered media (surrounding medium : black, inclusion A : blue and inclusion B : red.

TABLE II.II – Normalized range of the β parameter of the K-distribution over the three considered media in the dynamic mode.

Surrounding medium	Inclusion A	Inclusion B
2% agar- 3% gelatin	4% agar- 6% gelatin	4% agar- 4% gelatin
0.5326	0.8233	0.3457

II.5 Discussion

The current study suggests looking at the behavior of the statistical parameters under shear wave propagation for the purpose of tissue characterization. Previous reported*in-vitro* results from homogeneous agar-gelatin phantoms under transient shear wave propagation showed the time evolution of the β parameter of the K-distribution, which also presented a similar pattern as the displacement map [19]. For heterogeneous phantoms, we were motivated to see if the dynamic behavior of the β parameter of the echo envelope could give more information than its value in a static context. The above results seem to confirm this trend. First of all, the ultrasound echo envelope of random agar scatterers in gelatin was in good agreement with the K-distribution model fitting. Indeed, Figure II.2 shows the estimated PDF of the K-distribution for surrounding

agar gelatin and two hard inclusions, which were mimicking breast tumors. The same concentration of agar scatterers was chosen for the two inclusions. From its physical interpretation, the β parameter of the K-distribution is not only related to the density of the scatterers but also related to the medium (through the parameter α_0). Therefore, it was expected to obtain distinct values of the parameter for the two inclusions with different concentrations of gelatin in the static mode. According to Table II.I, the relative difference of β values between the surrounding medium and inclusions A and B were 65.4% and 6.4%, respectively, so that inclusion B was barely distinguished from the ambient medium. As a new step in tissue characterization, we were interested in the dynamic behavior of the β parameter under shear wave propagation. To have similar initial conditions, the distances of both inclusions from the rigid plate were the same. Table II.II presents the normalized range of the β parameter during shear wave propagation for the surrounding medium and the two inclusions. In the dynamic case, the relative difference between inclusions A, B and the surrounding medium were 35.3% and 35.1%, so that each inclusion was distinguished from the ambient medium. Moreover, the two inclusions could be distinguished with the normalized range of β (with relative difference of 58%)

II.6 Conclusion

Increasing the efficiency of ultrasound imaging remains a challenge in breast cancer diagnosis. Different statistical models and methods in the field of QUS have been proposed to develop quantitative tissue classification. This study provided an incentive for considering the dynamic behavior of statistical parameters of the ultrasound echo envelope under shear wave propagation to increase the power of standard QUS. Considering a breast mimicking phantom with two hard inclusions, we showed experimentally that the dynamic range of the statistical parameter β of the K-distribution could distinguish both inclusions from the surrounding medium, whereas the static values of this parameter could barely distinguish one of these inclusions from the surrounding medium.

II.7 Acknowledgment

This work was jointly supported by Collaborative Health Research grants from the Natural Sciences and Engineering Research Council of Canada (# 365656-09) and the Canadian Institutes of Health Research (CPG-95288).

II.8 References

1. Canadian Cancer Society, http ://www.cancer.ca/.

2. N. Mexico and A. Utah, "Relation of tumor size, lymph node status, and survival in 24,740 breast cancer cases," Cancer, 63, 181-187 (1989).

3. S. R. C. Benson, J. Blue, K. Judd and J. E. Harman, "Ultrasound is now better than mammography for the detection of invasive breast cancer," The American journal of surgery, 188, 381-385 (2004).

4. W. A. Berg, J. D. Blume, J. B. Cormack, E. B. Mendelson, D. Lehrer, M. Bohm-Velez, E. D. Pisano, R. A. Jong, W. P. Evans, M.J. Morton, M. C. Mahoney, L. H. Larsen, R. G. Barr, D. M. Farria, H. S. Marques and K. Bopara, "Combined screening with ultrasound and mammography vs mammography alone in women at elevated risk of breast cancer," JAMA : the journal of the American Medical Association, 299, 2151-2163 (2008).

5. K. I. Bland, E. M. Copeland. "The breast : Comprehensive management of benign and malignant disease," (Saunders Elsevier, 2009), Chap 11, pp. 231-243.

6. L. I. Petrella, H. de Azevedo Valle, P. R. Issa, C. J. Martins, J. C.Machado and W. C. Pereira "Statistical analysis of high frequency ultrasonic backscattered signals from basal cell carcinomas," Ultrasound in Med. & biol., 38, 1811-1819 (2012).

7. F. Destrempes and G. Cloutier, "A critical review and uniformized representation of statistical distributions modeling the ultrasound echo envelope," Ultrasound in Medicine & Biology, 36, 1037-1051 (2010).

8. P. M. Shankar, V. A. Dumane, J. M. Reid, V. Genis, F. Frosberg, C. W. Piccoli and B. Goldberg, "Classification of ultrasonic B-mode images of breast masses using Nakagami distribution," Ultrasonics, Ferroelectrics and Frequency Control, IEEE Transactions on, 48, 569-580 (2001).

9. M. L. Oelze, W. D. O'Brien, and J. F. Zachary, "Quantitative ultrasound assessment of breast cancer using a multiparameter approach," Proceedings of the 2007 IEEE Ultrasonics Symposium, 981-984 (2007).

10. K. J. Parker, M.M. Doyley, D.J. Rubens, "Imaging the elastic properties of tissue : the 20 year perspective," Physics in Medicine and Biology, 56, R1-R29 (2011).

11. J. Vappou, C. Maleke, E. E. Konofagou., "Quantitative viscoelastic parameters measured by harmonic motion imaging," Physics in Medicine and Biology, 54, 3579-3594 (2009).

12. Y. Y. Liao, C. H. Li, P. H. Tsui, C. C. Chang, W. H. Kuo, K. J. Chang and C. K. Yeh, "Strain-compounding technique with ultrasound Nakagami imaging for distinguishing between benign and malignant breast tumors," Medical Physics, 39, 2325-2333 (2012).

13. P. H. Tsui, C. Huang, Q. Zhou and K.K. Shung, "Cataract measurement by estimating the ultrasonic statistical parameter using an ultrasound needle transducer : an in vitro study," Physiological Measurement, 32, 513-522 (2011).

14. M. C. Ho, J. J Lin, Y. C. Shu, C. N. Chen, K. J. Chang, C. C. Chang and P. H. Tsui., "Using ultrasound Nakagami imaging to assess liver fibrosis in rats," Ultrasonics, 52, 215-222 (2012).

15. P. M. Shankar, J. M. Reid, H. Ortega, C. W. Piccoli, and B. B. Goldberg, "Use of non-Rayleigh statistics for the identification of tumors in ultrasonic B-scans of the breast", IEEE Trans. on Medical Imaging, 12, 687-692 (1993).

16. D. Blacknell and R. J. A. Tough, "Parameter estimation for the K-distribution based on [z log (z)]", IEE Proc. Radar, Sonar Navig., 148, 309-312 (2001).

17. V. Dutt and J. F. Greenleaf, "Ultrasound echo envelope analysis using a homodyned K distribution signal model," Ultrasonic Imaging, 16, 265-287 (1994).

18. G. Montaldo, M. Tanter, J. Bercoff, N. Benech, and M. Fink, "Coherent plane-wave compounding for very high frame rate ultrasonography and transient elastography," IEEE Trans. Ultrason. Ferroelectr. Freq. Control, 56, 489-506 (2009).

19. M. Alavi, F. Destrempes, C. Schmitt, E. Montagnon and G. Cloutier, "Shear wave propagation modulates quantitative ultrasound K-distribution echo envelope model statistics in homogeneous viscoelastic phantoms", Proceedings of the 2012 IEEE Ultrasonics Symposium, (2012).